

532
APR 6/77

MASTER

HA. 1454

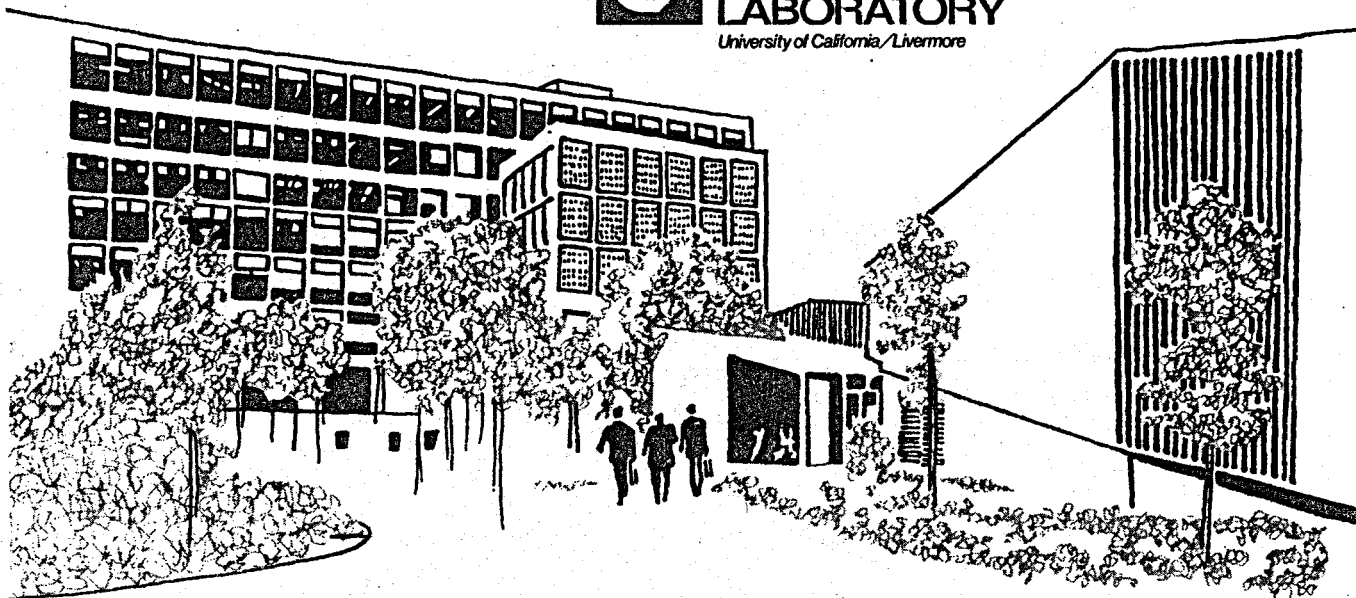
UCRL-52267

GEOLOGIC CHARACTERISTICS OF A PORTION OF THE SALTON SEA GEOTHERMAL FIELD

J. D. Tewhey

April 25, 1977

Prepared for U.S. Energy Research & Development
Administration under contract No. W-7405-Eng-48



DISTRIBUTION OF THIS DOCUMENT IS UNLIMITED

DISCLAIMER

This report was prepared as an account of work sponsored by an agency of the United States Government. Neither the United States Government nor any agency Thereof, nor any of their employees, makes any warranty, express or implied, or assumes any legal liability or responsibility for the accuracy, completeness, or usefulness of any information, apparatus, product, or process disclosed, or represents that its use would not infringe privately owned rights. Reference herein to any specific commercial product, process, or service by trade name, trademark, manufacturer, or otherwise does not necessarily constitute or imply its endorsement, recommendation, or favoring by the United States Government or any agency thereof. The views and opinions of authors expressed herein do not necessarily state or reflect those of the United States Government or any agency thereof.

DISCLAIMER

Portions of this document may be illegible in electronic image products. Images are produced from the best available original document.

NOTICE

This report was prepared as an account of work sponsored by the United States Government. Neither the United States nor the United States Energy Research & Development Administration, nor any of their employees, nor any of their contractors, subcontractors, or their employees, makes any warranty, express or implied, or assumes any legal liability or responsibility for the accuracy, completeness or usefulness of any information, apparatus, product or process disclosed, or represents that its use would not infringe privately-owned rights.

Printed in the United States of America
Available from
National Technical Information Service
U.S. Department of Commerce
5285 Port Royal Road
Springfield, VA 22161
Price: Printed Copy \$; Microfiche \$3.00

Page Range	Domestic Price	Page Range	Domestic Price
001-025	\$ 3.50	326-350	10.00
026-050	4.00	351-375	10.50
051-075	4.50	376-400	10.75
076-100	5.00	401-425	11.00
101-125	5.50	426-450	11.75
126-150	6.00	451-475	12.00
151-175	6.75	476-500	12.50
176-200	7.50	501-525	12.75
201-225	7.75	526-550	13.00
226-250	8.00	551-575	13.50
251-275	9.00	576-600	13.75
276-300	9.25	601-up	*
301-325	9.75		

*Add \$2.50 for each additional 100 page increment from 601 to 1,000 pages;
add \$4.50 for each additional 100 page increment over 1,000 pages.

Distribution Category
UC-66a



LAWRENCE LIVERMORE LABORATORY
University of California, Livermore, California, 94550

UCRL-52267


GEOLOGIC CHARACTERISTICS OF A PORTION OF THE SALTON SEA GEOTHERMAL FIELD

J. D. Tewhey

MS date: April 25, 1977

NOTICE

This report was prepared as an account of work sponsored by the United States Government. Neither the United States nor the United States Energy Research and Development Administration, nor any of their employees, nor any of their contractors, subcontractors, or their employees, makes any warranty, express or implied, or assumes any legal liability or responsibility for the accuracy, completeness or usefulness of any information, apparatus, product or process disclosed, or represents that its use would not infringe privately owned rights.

DISTRIBUTION OF THIS DOCUMENT IS UNLIMITED 

Contents

List of Illustrations	iv
List of Tables	vi
Abstract	1
Introduction	2
The Cap Rock	7
Unaltered Reservoir Rocks	11
Hydrothermally Altered Reservoir Rocks	16
Theoretical Aspects of the Alteration Scheme	16
Characteristics of Hydrothermally Altered Reservoir Rocks	21
The Effects of Alteration on Reservoir Properties.	27
The Significance of Fracture Porosity and Permeability	31
Well Log Correlation	32
A Comparison of Two Geothermal Wells	37
Acknowledgments	39
References	40
Appendix A: The Construction and Use of Activity Diagrams	43
Appendix B: Tables of Chemical Analyses	47
Appendix C: Porosity Measurements of Core Samples	51

List of Illustrations

Figure	Title	Page
1.	Location of the Salton Sea geothermal field and nearby faults in Imperial Valley.	3
2.	Cross section of the Salton Trough and the Salton Sea geothermal field.	4
3.	Well locations in the Salton Sea geothermal field.	5
4.	The three general rock categories in the sedimentary sequence of the Salton Sea geothermal field.	6
5.	Lithologic logs of cap rock compiled on the basis of drill cuttings samples.	8
6.	Fine-grained massive anhydrite from Magmamax 2; depth, 970 ft (290 m).	9
7.	Coarse-grained anhydrite from Magmamax 3; depth, 870 ft (265 m)	9
8.	Coarse-grained anhydrite in a carbonate matrix from Magmamax 2; depth, 820 ft (250 m).	10
9.	The abundance of pyrite in drill cuttings from the Magmamax 2 and 3 wells.	13
10.	Photomicrographs of unaltered calcareous sandstone from the 1240- to 1270-ft (378- to 388-m) interval in Magmamax 2.	14
11.	Unaltered shale from the 2000- to 2060-ft (610- to 630-m) interval in Magmamax 2.	15
12.	X-ray diffraction patterns of unaltered sandstone and unaltered shale from Magmamax 2.	16
13.	Activity diagrams showing phase relations in the Salton Sea geothermal system.	18
14.	The $\text{CaO-Al}_2\text{O}_3\text{-SiO}_2\text{-H}_2\text{O}$ system. (a) Mineral composition. (b) Temperature-mole fraction CO_2 plot at $P_{\text{fluid}} = 2$ kbar.	20
15.	Alteration zone contours. (a) The top of the metamorphic zone in the Salton Sea geothermal field as determined by electric logs. (b) The top of the zone of alteration as determined in this study by the first appearance of epidote in drill cuttings.	22

Figure	Title	Page
16.	Hydrothermally altered sandstones from the 4340-ft (1323-m) level (TD) in Magmamax 2.	23
17.	Mineral compositions. (a) Compositions plotted on the projection plane of an AFKM (Thompson) projection. (b) Range of chlorite and biotite compositions in a single sample from the 4340-ft (1323-m) level (TD) in Magmamax 2.	25
18.	Results of microprobe analysis of zoned epidote grains from the 4340-ft (1323-m) level in Magmamax 2.	26
19.	Thin section photomicrographs of epidote grains in a sample from 4340-ft (1323-m) level (TD) in Magmamax 2.	26
20.	Well-formed epidote crystals in partially filled fracture in shale.	27
21.	Large fracture in shale completely filled with anhydrite.	28
22.	Plot of porosity vs depth for cores from Woolsey 1 and State of California 1 wells.	29
23.	East-west cross section through the Magmamax and Woolsey wells depicting directional mode of porosity gradients.	30
24.	Calcite vein in shale from the 3630-ft (1110-m) level in Magmamax 2.	31
25.	Calcite-epidote vein in shale from the 3820-ft (1167-m) level in Magmamax 3.	32
26.	Spontaneous potential log correlation of the Magmamax and Woolsey wells.	34
27.	Detail of electric log and corresponding lithology over the interval 2400 to 2650 ft (730 to 810 m) in Woolsey 1.	35
28.	Correlation of SP log and drill cuttings analysis.	36
29.	Magmamax and Sinclair well comparisons.	38
A1.	Reaction curves for the systems $K_2O-Al_2O_3-SiO_2-H_2O$ and $Na_2O-Al_2O_3-SiO_2-H_2O$	45
A2.	Mineral stability relations in the system $K_2O-Na_2O-Al_2O_3-SiO_2-H_2O$ at 300°C and approximately 1 kbar.	46
B1.	Epidote grains contoured in Fig. 19.	49

List of Tables

Table	Title	Page
B1.	Chemical analysis of chlorite from 4340-ft (1420-m) depth in Magmamax 2.	47
B2.	Chemical analysis of biotite from 4340-ft (1420-m) depth in Magmamax 2.	48
B3.	Chemical analysis of feldspar from 4340-ft (1420-m) depth in Magmamax 2.	49
B4.	Selected epidote analyses from 4340-ft (1420-m) depth in Magmamax 2.	50
C1.	Porosity measurements of core samples from Woolsey No. 1 and State of California No. 1.	51

GEOLOGIC CHARACTERISTICS OF A PORTION OF THE SALTON SEA GEOTHERMAL FIELD

Abstract

The examination of drill cuttings and core samples from the Magmamax Nos. 2 and 3 and Woolsey No. 1 wells indicate that the sequence of sedimentary rocks in the Salton Sea geothermal field from the surface to below 4000 ft (1200 m) can be divided into three categories: (1) cap rock, (2) unaltered reservoir rocks, and (3) hydrothermally altered reservoir rocks. The cap rock extends from the surface to a depth of approximately 1100 ft (350 m) in all three wells. The uppermost 600 ft (200 m) of the cap rock consists of unconsolidated silt, sand, and gravel. The interval from 600 to 1100 ft (200 to 350 m) consists of anhydrite-rich evaporites in a carbonate-clay matrix and has low permeability. There is evidence to suggest that the cap rock has undergone self-sealing through time as a result of the circulation of hot brine through the rocks. Essentially unaltered reservoir rocks extend from a depth of 1100 ft (350 m) to approximately 3000 ft (900 m). The sequence consists principally of well-indurated shales, siltstones, and sandstones consisting of clastic quartz and feldspar grains cemented

with calcite and/or silica. The mineralogical and textural changes that occur at depth can be attributed to the process of hydrothermal alteration. Alteration has occurred in a chemically open system and the important variables in the alteration scheme have been temperature, permeability, brine composition, and rock composition. The transition from unaltered to altered reservoir rocks is marked by the replacement of calcite by epidote. The first appearance of epidote correlates reasonably well with the top of the alteration zone as determined in other studies by electric log analysis. Biotite and chlorite, potential indicators of alteration zones, are considered to be of detrital origin rather than hydrothermal origin. The primary effect of hydrothermal alteration on the reservoir rocks in the Salton Sea geothermal field has been the reduction of porosity and permeability with depth. Petrographic analysis indicates that porosity and permeability in the field is enhanced by the presence of fractures in shales. Spontaneous potential (SP) log correlation is possible for the wells

studied and the geologic picture that emerges from the correlation scheme is that of a structural basin whose axis lies to the northwest of Magmamax No. 2. Geothermal production characteristics vary with depth and position in the

field as a result of temperature, salinity, and porosity/permeability gradients in the reservoir. The data suggests that unaltered reservoir rocks on the periphery of the field offer good production possibilities.

Introduction

It has been determined on the basis of geological¹ and geophysical evidence² that the sequence of sedimentary rocks in the Salton Trough is approximately 20,000 ft (6000 m) thick. Field work in the folded sedimentary rocks along the margins of the trough¹ and the examination of cuttings from the 13,443 ft (4097 m) Wilson No. 1 well near Brawley indicate that the entire 20,000 ft (6000 m) sequence is composed of detritus from the Colorado River.³ Only minor contributions appear to have come from the Chocolate Mountains and peninsular ranges that border the trough. Unaltered deltaic sediments in the Salton Trough have a rather uniform composition consisting predominantly of quartz and calcite with subordinate amounts of dolomite, feldspar, clay minerals, mica, and the common accessory minerals.³ Data from the present study and several previous ones^{1,4,5} have been compiled to make a geologic map and cross section of

the Salton Trough that includes the Salton Sea geothermal field (Figs. 1 and 2).

The present study is based on the examination of drill cutting samples from three wells located in the west-central portion of the Salton Sea geothermal field: Magmamax Nos. 2 and 3 and Woolsey No. 1 (Fig. 3). The Magmamax Nos. 2 and 3 wells were drilled to total depths of 4368 ft (1331 m) and 4000 ft (1219 m), respectively, in 1972. Woolsey No. 1 was drilled to a depth of 2400 ft (731.5 m) in 1972 and deepened to 3490 ft (1064 m) in January 1977. At the time of deepening Woolsey No. 1, core samples were taken over the intervals 2565 to 2605 ft (782 to 794 m) and 3417 to 3437 ft (1041.5 to 1048 m). All three wells were drilled by the Magma Power Company for geothermal purposes. The detailed history and characteristics of these and other wells in the Salton Sea geothermal field can be found in Ref. 6.

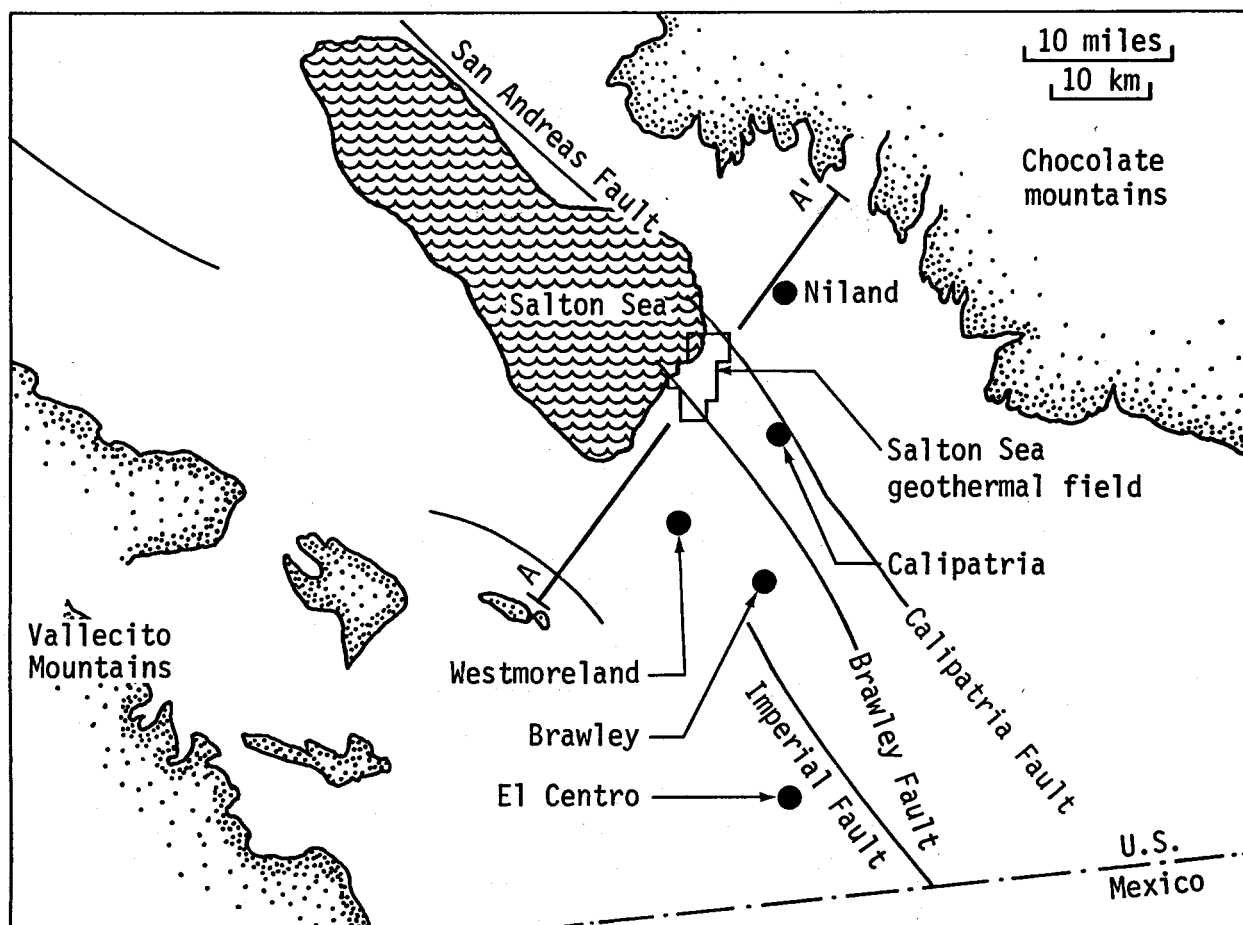


Fig. 1. Location of the Salton Sea geothermal field and nearby faults in Imperial Valley (modified from Ref. 4). Basement rocks are indicated by the stippled pattern. The cross section in Fig. 2 is drawn across line A-A'.

All of the cutting samples from the three wells were examined microscopically. Specific samples were selected for petrographic, x-ray diffraction, and microprobe analysis. Porosity measurements and petrographic analysis were done on core samples from the Woolsey No. 1 and State of California No. 1 wells. The observations recorded, analytical data gathered, and conclusions drawn are presented herein.

In terms of an overview, the drill cutting data indicates that the sedimentary sequence in the study area from the surface to below 4000 ft (1200 m) can be divided into three categories: (1) cap rock, (2) essentially unaltered reservoir rocks, and (3) hydrothermally altered reservoir rocks. The division of categories as a function of depth for the wells studied is shown schematically in Fig. 4.

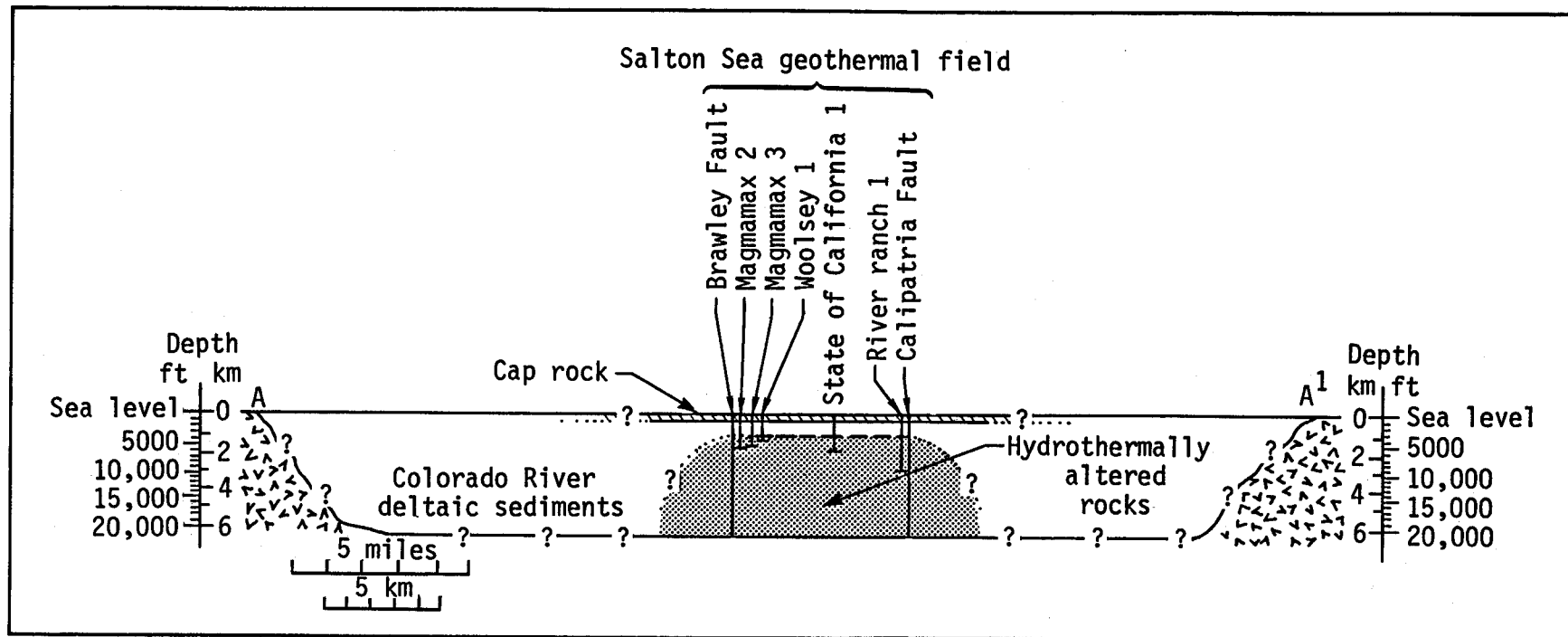


Fig. 2. Cross section of the Salton Trough and the Salton Sea geothermal field. There is no vertical exaggeration.

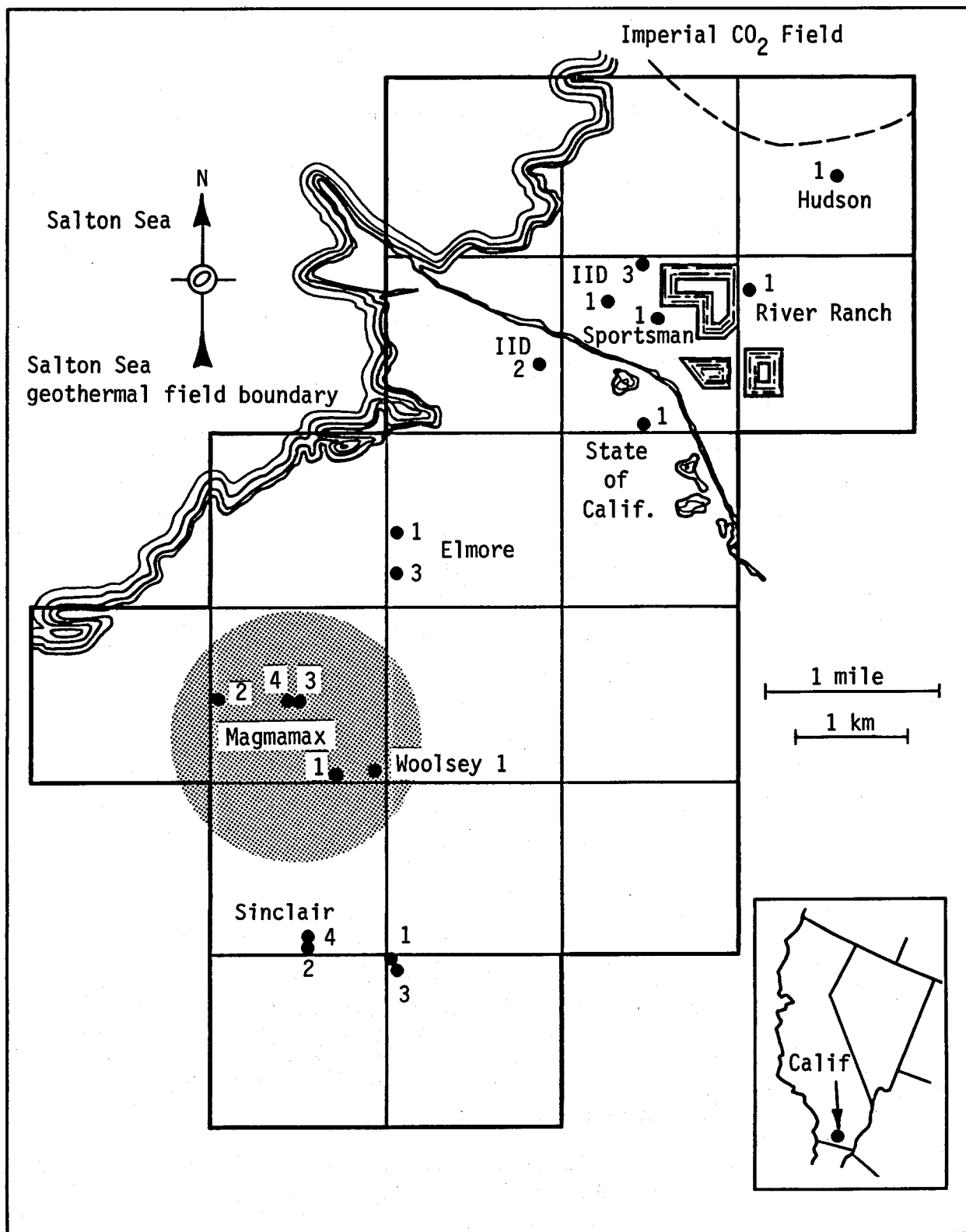


Fig. 3. Well locations in the Salton Sea geothermal field. The shaded area is the region investigated in this report.

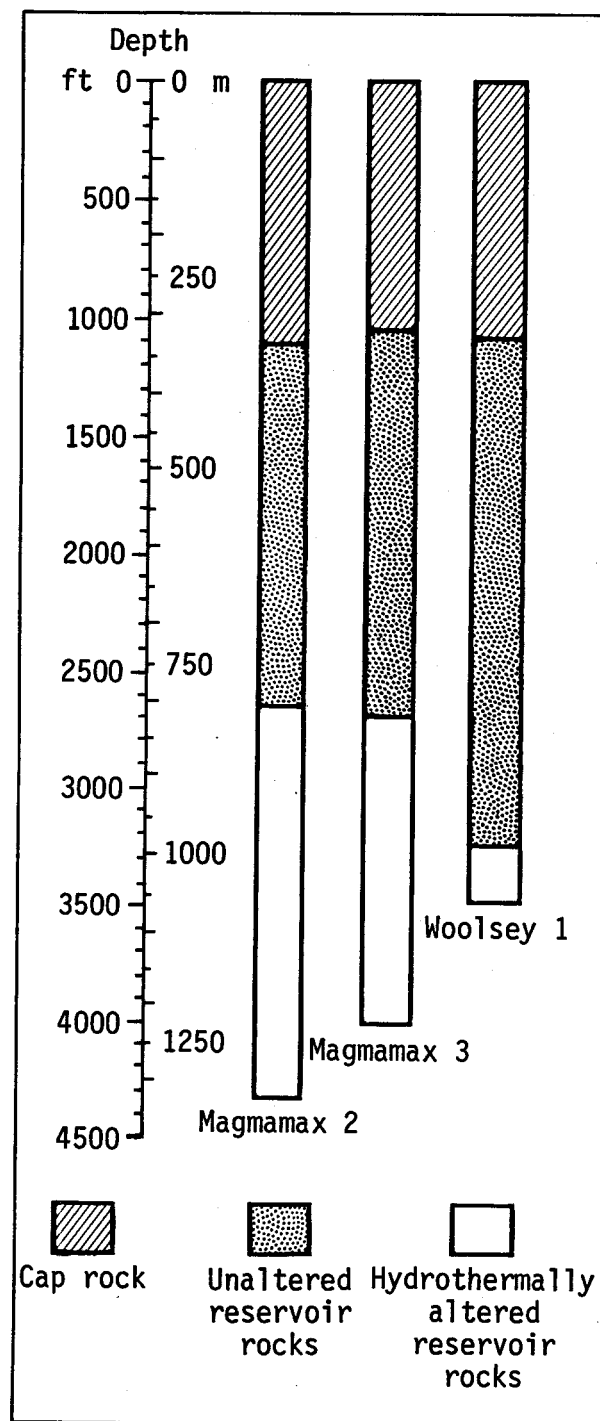


Fig. 4. The three general rock categories in the sedimentary sequence of the Salton Sea geothermal field.

The Cap Rock

The cap rock of a geothermal system is the thick layer of low-permeability rock that overlies or caps the more permeable reservoir rocks. It is analogous to a lid on a boiling pot. First, it serves as a limiting barrier for circulating convection currents, preventing them from dissipating heat and discharging fluids at the surface. Second, it has the potential for serving as a thermal insulator, allowing heat to be retained in the reservoir and thereby contributing to the buildup of temperature in the geothermal system.

There has been no detailed study of the lithologic units that make up the cap rock of the Salton Sea geothermal system, although the rocks encountered in the upper parts of geothermal wells have been treated in a general way in a number of papers dealing with the geology of the Salton Trough. The uppermost sequence of rocks in the area has been described as:

- A hard, dense shale-siltstone-clay section that attains a thickness of 2000 to 3000 ft (600 to 900 m).⁷
- A partially consolidated clay-silt-evaporite series.⁵

On the basis of observations of drill cutting samples from three

wells, I feel that the latter is the more appropriate cap rock description. Hard, dense shales and siltstones are present in the lithologic column but occur below a distinct boundary between the cap rock and the underlying reservoir rocks. Also, petrographic analysis indicates that the shales and siltstones underlying the cap rock have appreciable fracture permeability, thereby limiting their effectiveness as aquitards.

In the vicinity of the Magmamax wells, Randall⁵ and Towse and Palmer⁸ have determined on the basis of log analyses that the reservoir rocks occur at relatively shallow depths, the top of the sandstone section being at a depth of 1100 to 1200 ft (340 to 370 m). The existence of reservoir rocks at shallow depths in that area is supported by analyses of drill cutting samples. On the basis of these observations, the cap rock in the southwestern portion of the geothermal field can be limited to the sequence of sediments extending from the surface to a depth of 1100 ft (350 m).

Drill cutting samples taken at 30-ft intervals were analyzed from the Magmamax 2 and 3 and Woolsey 1 wells. The results of the sample analysis for the cap rock are presented schematically in Fig. 5.

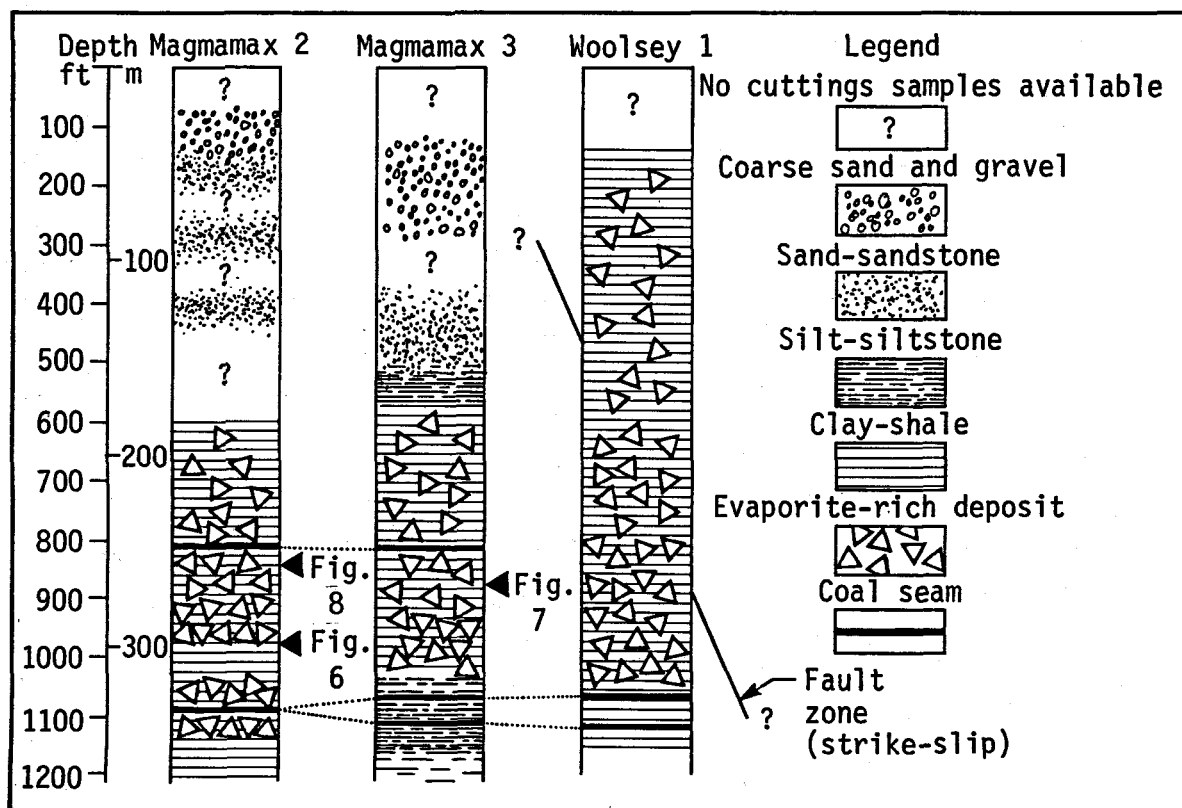


Fig. 5. Lithologic logs of cap rock compiled on the basis of drill cuttings samples. Locations of samples shown in Figs. 6 to 8 are indicated. Samples were taken every 30 ft.

It should be pointed out that the inherent difficulties in working with drill cutting samples are:

- Local and/or subtle differences in lithology tend to be "smoothed out."
- Contamination of samples can occur by sloughing of material from above the interval being drilled.
- The fine-grained components of loosely consolidated sedimentary rocks tend to become suspended in the drilling fluid and are not collected in the cuttings sample, thereby re-

sulting in a sample that is not representative of the formation.

As a result of these problems, the data presented in Fig. 5 should be interpreted as a representation of the gross features of the lithologic section. Any subtle and/or local variations in the section may not have been detectable by means of cuttings analysis.

The cuttings samples indicate that the material in the uppermost 600 ft (200 m) of the Magmamax wells consists of unconsolidated silt, sand, and gravel. Van de Kamp⁹ has found

that near-surface cores taken within the Salton basin invariably contain considerable amounts of lacustrine mud. Also, the drilling logs from 11 geothermal wells in the Salton Trough indicate abundant clay at shallow depths. Therefore, it is probable that the cutting samples from Magmamax 2 and 3 have been depleted in fine-grained components in the process of drilling and sample acquisition. With a clay-silt matrix, the near-surface sediments would have low permeability and, therefore, would be considered a viable cap rock.

The portion of the lithologic section depicted in Fig. 5 that appears to fulfill the function of a cap in the strict sense is the 500-ft interval between the depths of 600

and 1100 ft (200 to 350 m). This interval consists primarily of anhydrite-rich evaporites, varietal forms of which are fine-grained massive anhydrite (Fig. 6), coarse-grained anhydrite (Fig. 7), or anhydrite crystals in a carbonate and/or clay matrix (Fig. 8). All of these rocks are consolidated and are not readily friable. These photomicrographs show that the evaporites have textures consisting of interlocking grains, a feature that contributes to low permeability.

The presence of anhydrite in the cap rock is in agreement with thermodynamic predictions. Gypsum is a common precipitate from sea water, but its stability field is limited



Fig. 6. Fine-grained massive anhydrite from Magmamax 2; depth, 970 ft (290 m). Cross polarizers, 350× magnification.

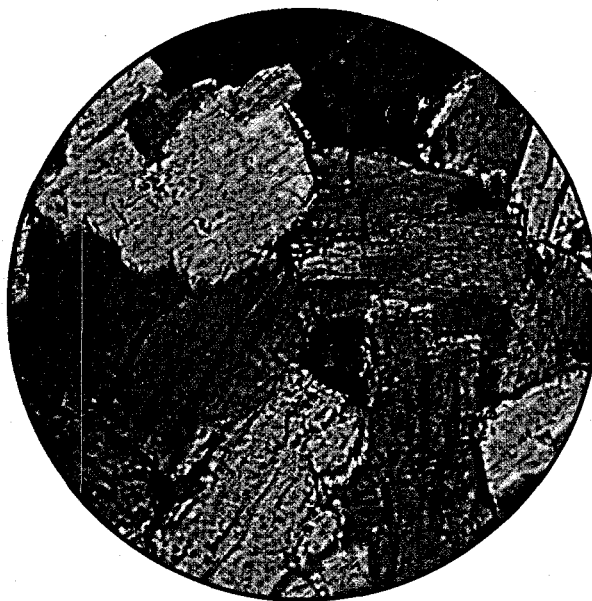


Fig. 7. Coarse-grained anhydrite from Magmamax 2; depth, 870 ft (265 m). Crossed polarizers, 140× magnification.

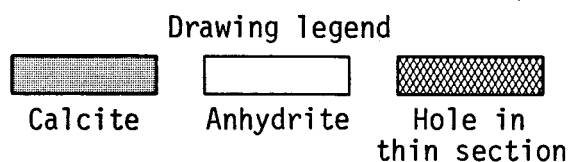
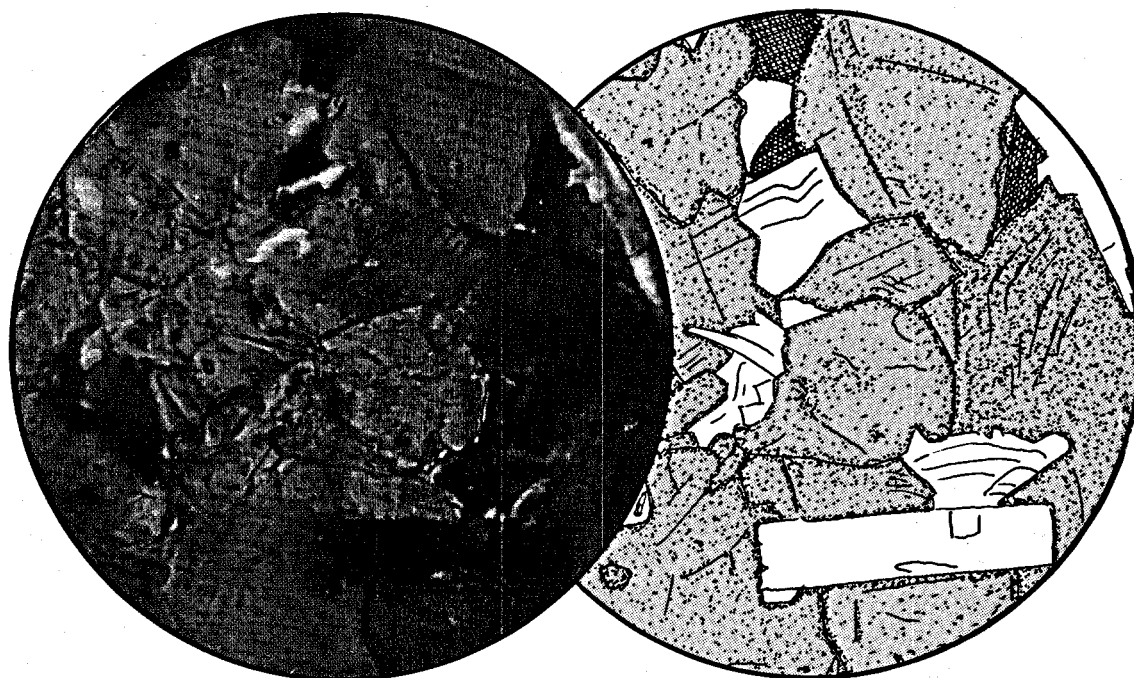


Fig. 8. Coarse-grained anhydrite in a carbonate matrix from Magmamax 2; depth, 820 ft (250 m). Crossed polarizers, 400X magnification (left); drawing of same (right). (The holes in this and later thin sections were knocked out by the grinding operation in making the sections.)

to surface and near-surface environments. During burial and diagenesis, gypsum undergoes dehydration and is converted to anhydrite.¹⁰ The relatively thick sequence of evaporite-rich deposits in the Salton basin are indicative of the long sequence of intermittent "Salton Seas" that have existed in the past.

There is an apparent lack of correlation between the uppermost portions of the Woolsey and Magmamax

wells. One way of accounting for the discrepancy is to assume that a fault is present in the vicinity of the Woolsey well (see Fig. 5). To explain substantial differences in the thickness of the cap rock in adjacent wells, Randall⁵ has postulated the existence of numerous right-lateral strike-slip faults in the Salton Trough with offsets of 1 km or more. Strike-slip movement, which is in accord with the plate

tectonic regime of the Salton Trough, can be used to account for the apparent vertical movement of the cap rock in that the cap rock is roughly wedge-shaped, thickening toward the west and thinning toward the north, east, and south.⁷

At the bottom of the cap rock sequence there appears to be good stratigraphic correlation between the three wells as indicated by the thin coal seams that serve as marker horizons. Shallow coal seams are common in the Salton Trough and are usually referred to as carbonaceous material or lignite on the drilling logs.

Facca and Tonani¹¹ have theorized and showed empirically that hot water circulating in a hydrothermal system can produce alteration and deposition along flow paths in the cap rock, thereby reducing permeability. In this manner, a geothermal system can be self-sealing by producing and/or restoring its own cap rock. There are several lines of evidence suggesting that the cap rock associated with the Salton Sea geothermal field has been self-sealing. Direct evidence of self-sealing phenomena in the

vicinity of the Salton Sea is provided by Batzle and Simmons,¹² who have examined samples of cap rock from the Dunes area of the Salton Trough with a scanning electron microscope. They interpret minute veinlets and fluid inclusion trains to be microcracks that have been "healed" by the precipitation of minerals from circulating fluids. Less-direct evidence of self-sealing comes from the thermal spring activity in the area, which tends to be concentrated along the traces of fault-induced linements.¹³ Early reports¹⁴ indicate that considerable thermal spring and geyser activity took place in what is now the Salton Sea geothermal area. The current discharge rate from feeble hot springs probably does not exceed 20 gal/min,¹³ ostensibly indicating that cap rock perforations along fault planes have been gradually sealed through time. There is evidence to suggest that the process of crack production and subsequent sealing is not limited to the cap rock but occurs in reservoir rocks as well. This will be discussed further in a later section.

Unaltered Reservoir Rocks

Technically, there are no unaltered sediments in the cuttings

examined as part of this study. The presence of thermal springs at the

surface indicate that hot brines have penetrated the entire sedimentary section, and it is reasonable to expect that they have permeated the rocks along the route to the surface whenever they have been able to do so. The brine-induced alteration effects in the uppermost reservoir rocks are principally silicification and clay mineral reactions. An example of the latter is the reaction in which kaolinite and montmorillonite are transformed to chlorite and/or illite.^{13,15}

With the exception of pyrite mineralization, discussed below, the alteration of rocks above 2700 ft (800 m) in the Magmamax wells and above 3300 ft (1000 m) in the Woolsey well is subtle enough to be detectable only by means of careful x-ray diffraction analysis or detailed petrographic studies. The point to be emphasized is that these alteration effects have not changed the *petrophysical properties* (e.g., porosity and permeability) of the reservoir rocks any more than that normally expected during the process of lithification via burial diagenesis. The geochemist or petrologist who specializes in hydrothermal alteration schemes would refer to these rocks as being moderately altered.¹⁶ However, for the sake of differentiating between the uppermost reservoir rocks and the deeper ones

that exhibit alteration of petrophysical properties, the terms "unaltered" and "altered" will be used here.

The first appearance of epidote has been used to mark the transition from unaltered to altered rock. The epidote isograd corresponds reasonably well with the "top of the metamorphic zone" as determined by Randall⁵ through log analysis.

Pyrite is present at all depths in the three wells, and the ubiquity of sulfide mineralization throughout the geothermal field is attested by Skinner *et al.* (p. 324),¹⁷ by Helgeson (p. 135),⁷ and by the drilling logs compiled by numerous well-site geologists. Figure 9 shows the manner in which pyrite is distributed in the Magmamax wells. The upper salient represents the distribution in the cap rock; the lower salient, which builds up gradually over a 2000-ft interval, represents the distribution in the reservoir rocks. As indicated by the sketches in Fig. 9, the pyrite in the reservoir rocks occurs as fresh, well-formed crystals that fill voids; there is little doubt that they are hydrothermal in origin. On the other hand, the pyrite in the near-surface environment is fine-grained, massive, and black-brass in color and is interpreted as being a normal product to diagenesis in sulfidic cap rock sediments. Helgeson

(p. 135)⁷ shows a similar distribution of pyrite (plus epidote and hematite) for the IID well No. 2.

The sharp transition between the cap rock and the underlying sequence of unaltered clastic sediments probably represents the lower boundary of the Brawley Formation of Pleistocene age. The interface has been interpreted as an unconformity by Randall (p. 44)⁵ on the basis of structural arguments, whereas earlier workers^{1,18} have considered the entire Miocene-Pleistocene sequence in the Salton Trough as being conformable. In the Magmamax Nos. 2 and 3 wells, the zone of unaltered reservoir rocks is about 1600 ft (490 m) thick, extending from a depth of about 1100 ft (340 m) to nearly 2700 ft (820 m). In Woolsey No. 1, the zone of unaltered rocks is nearly 2200 ft (670 m) thick, extending from about 1100 ft (340 m) to nearly 3300 ft (1000 m). The eastward thickening of the zone of unaltered rocks over the study area is a result of the gradually increasing depth to the zone of altered rocks over the same interval. This phenomenon is related to the heat distribution in the geothermal field and has been described and documented by Randall⁵ and will be discussed in more detail in a later section.

The unaltered sequence in the Magmamax and Woolsey wells consist

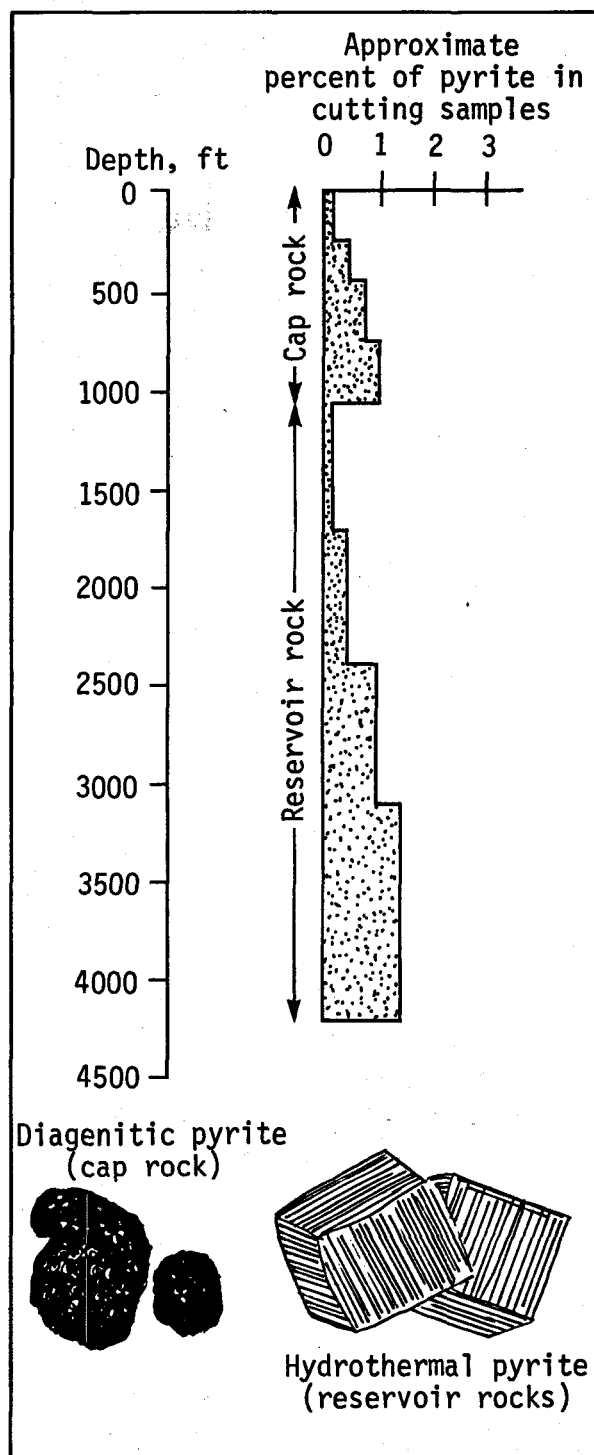
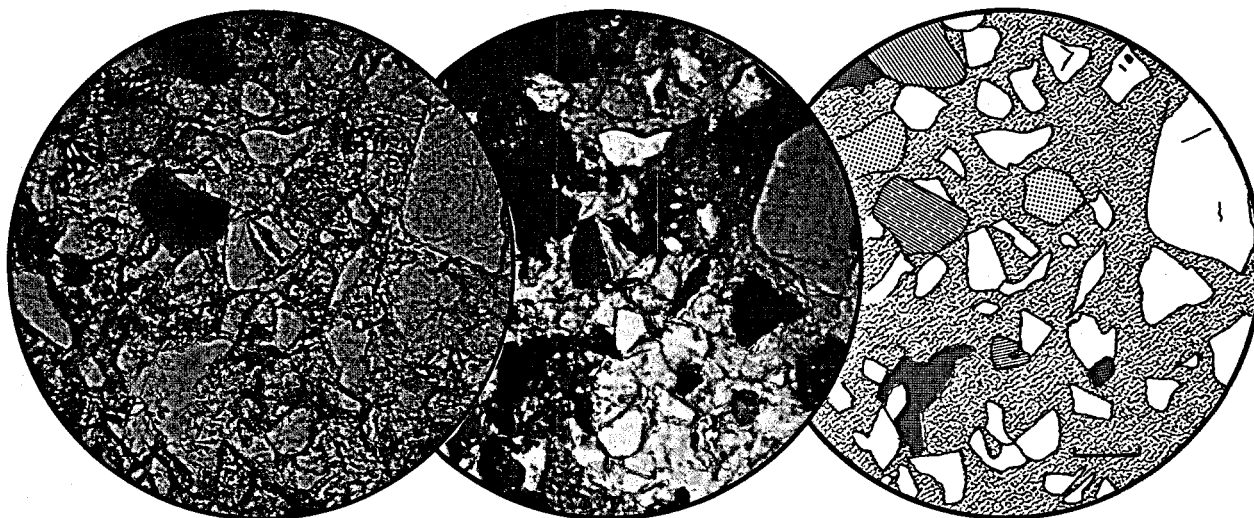


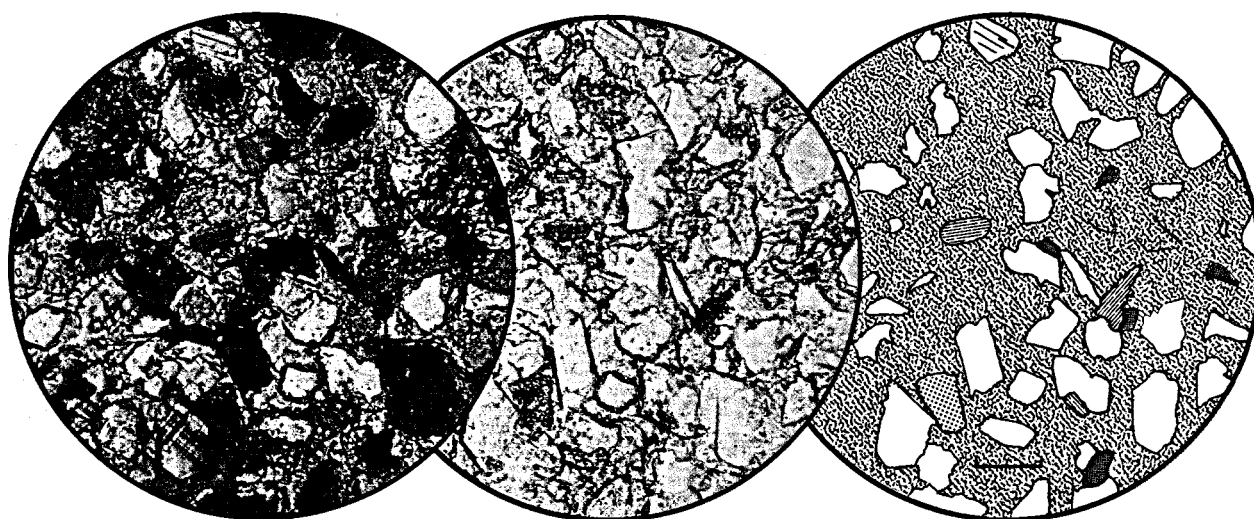
Fig. 9. The abundance of pyrite in drill cuttings from the Magmamax 2 and 3 wells. The sketches indicate the form of the pyrite crystals in the cap rock and reservoir rocks.



Crossed polarizers

Plane-polarized light

Drawing



Crossed polarizers

Plane-polarized light

Drawing

Drawing legend



Quartz



Feldspar



Calcite



Biotite



Chlorite



Lithic
fragment

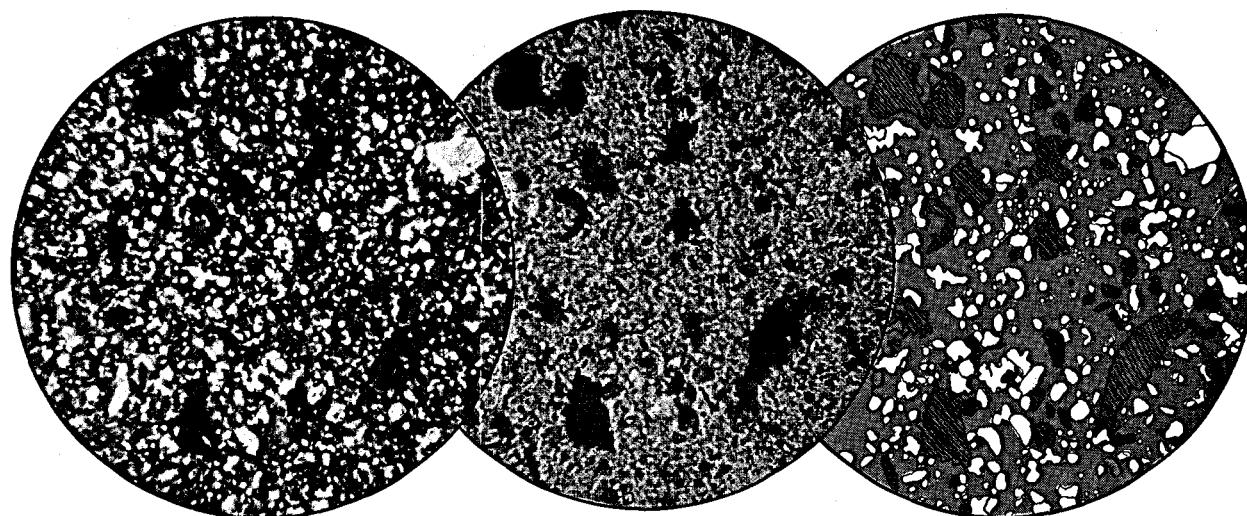


Hole in
thin section

Fig. 10. Photomicrographs of unaltered calcareous sandstone from the 1240- to 1270-ft (378- to 388-m) interval in Magmamax 2. 120 \times magnification (scale bar in drawings = 0.1 mm).

of indurated sandstones, siltstones, shales, and a few thin coal seams. Annotated photomicrographs of calcareous sandstones and a shale from the unaltered zone in Magmamax 2 are shown in Figs. 10 and 11. The sandstone consists of subangular clastic grains of quartz with minor feldspar, mica, chlorite, and lithic fragments. The rocks are well-cemented with calcite, and interstitial pores are not readily apparent in thin sections of these particular samples. Other sandstone specimens in the unaltered sequence

exhibit porosities of greater than 20%. The mineral assemblage of the fine-grained shale (Fig. 11) is best determined by means of its x-ray diffraction pattern, shown in Fig. 12. The x-ray analysis indicates the presence of quartz, calcite, chlorite, illite, mica, and feldspar. The chlorite and illite are considered to be hydrothermal alteration products derived from precursor kaolinite and/or montmorillonite. The brown specks of material evident in the thin section photomicrograph are bits of organic debris.



Crossed polarizers

Plane-polarized light

Drawing

Drawing legend

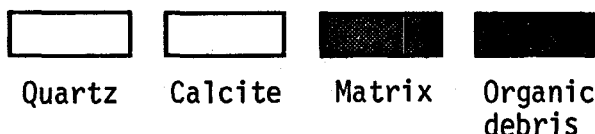


Fig. 11. Unaltered shale from the 2000- to 2060-ft (610- to 630-m) interval in Magmamax 2. 305× magnification (scale bar adjacent to drawing = 0.05 mm).

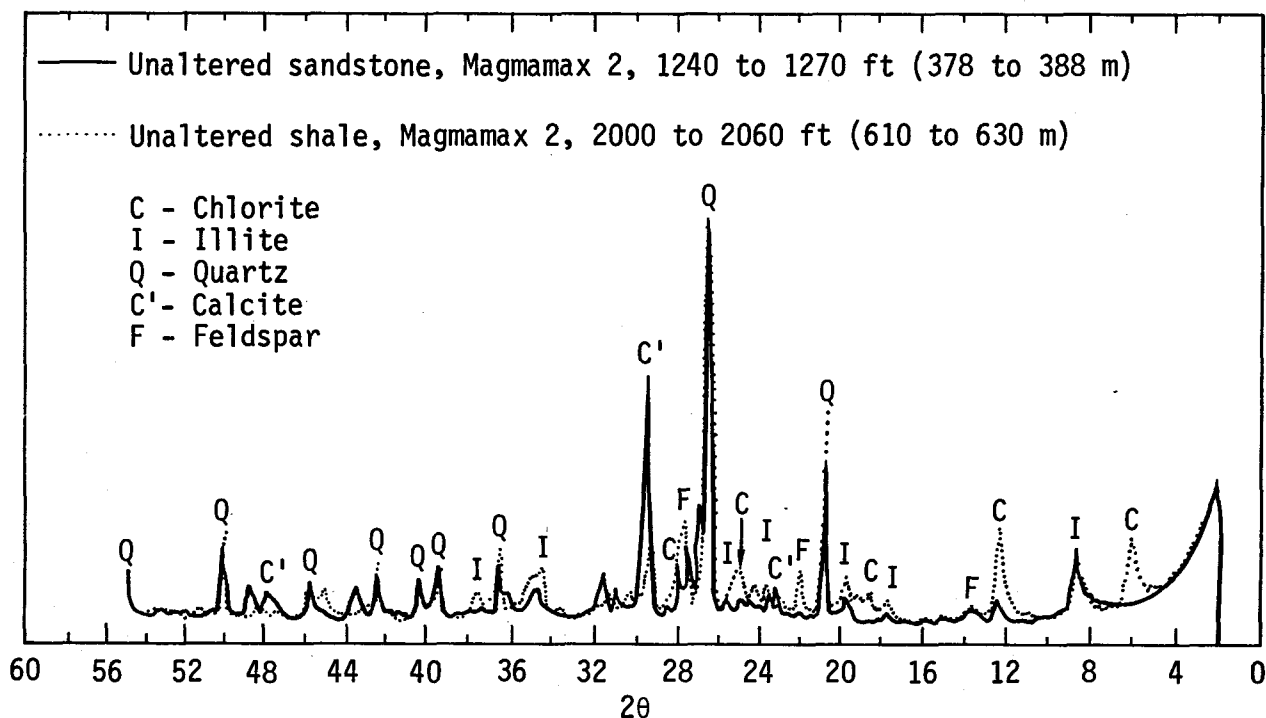


Fig. 12. X-ray diffraction patterns of unaltered sandstone and unaltered shale from Magmamax 2. Photomicrographs are shown in Figs. 10 and 11, respectively.

Hydrothermally Altered Reservoir Rocks

THEORETICAL ASPECTS OF THE ALTERATION SCHEME

The mineralogical and textural changes that occur in rocks at depth in the Salton Sea geothermal field can be attributed to the process of hydrothermal alteration. On the basis of previous geological studies in the Salton Trough^{3,16} and the petrographic analyses done as part of this study, it appears to be a reasonable assumption that the mineralogy of the altered reservoir

rocks was originally similar to that of the overlying sequence of unaltered rocks discussed earlier. It is clear that the mineralogical changes that have occurred in going from the unaltered to the altered sequence of rocks have not been isochemical. Hydrothermal alteration has occurred in an open system and there has been significant mass transfer of chemical constituents during the process. The important variables in the alteration scheme appear to have been temperature, brine composition,

and the original rock composition. Within the temperature range of the Magmamax wells ($<300^{\circ}\text{C}$), rock permeability is also an important variable. Sandstones and siltstones exhibit appreciable alteration as a result of being infiltrated by hot, high-salinity brines, whereas the less-permeable shales show relatively minor effects. Heat-induced textural and mineralogical changes (i.e., metamorphism) are likely to be encountered in shales in the deeper portions of the reservoir and would tend to make the alteration effects resulting from permeability differences less conspicuous.

Helgeson (p. 362)¹⁹ has pointed out the dichotomy that has evolved in the manner in which petrologists and geochemists study metamorphic processes. The petrologist tends to think in terms of solid-phase equilibria, emphasizing *rock* composition as a primary variable, whereas the aqueous geochemist tends to think in terms of rock-water interactions, emphasizing *fluid* composition as a primary variable. In studies of ancient metamorphic terrains, the petrologist's view tends to prevail in the literature because little can be determined about the fluid phase that might have been present during metamorphism. In areas of "active metamorphism" such as the Salton Sea geothermal field, much can be learned

about the fluid phase coexisting with the rocks; therefore, it is reasonable to express mineral stabilities in terms of fluid compositions.

Phase diagrams that depict mineral stability fields in terms of temperature and chemical composition of the coexisting aqueous fluid were developed by Hemley,²⁰ Hemley and Jones,²¹ and Helgeson¹⁹ and have been used in a number of geothermal-related studies. Hemley-Helgeson diagrams — or, more simply, activity diagrams — for the Mg-Ca-H and Na-K-H systems are shown in Fig. 13. Two sets of stability field boundaries have been drawn on each plot; the dotted lines denote the stability fields at 250°C , the solid lines at 300°C . The former is representative of conditions in the production zone of Magmamax 1; the latter, the production zone in Sinclair 4. These two wells were chosen because of (1) the availability of brine analyses and (2) the significant temperature differences in the two production zones. The open and solid circles represent the brine chemistry of Magmamax 1 and Sinclair 4, respectively. The diagrams indicate the brine in Magmamax 1 is compatible with a low-grade clay mineral assemblage, whereas the brine from the deeper and hotter Sinclair 4 well is compatible with a higher grade chlorite-feldspar assemblage. Note that neither of the two brines

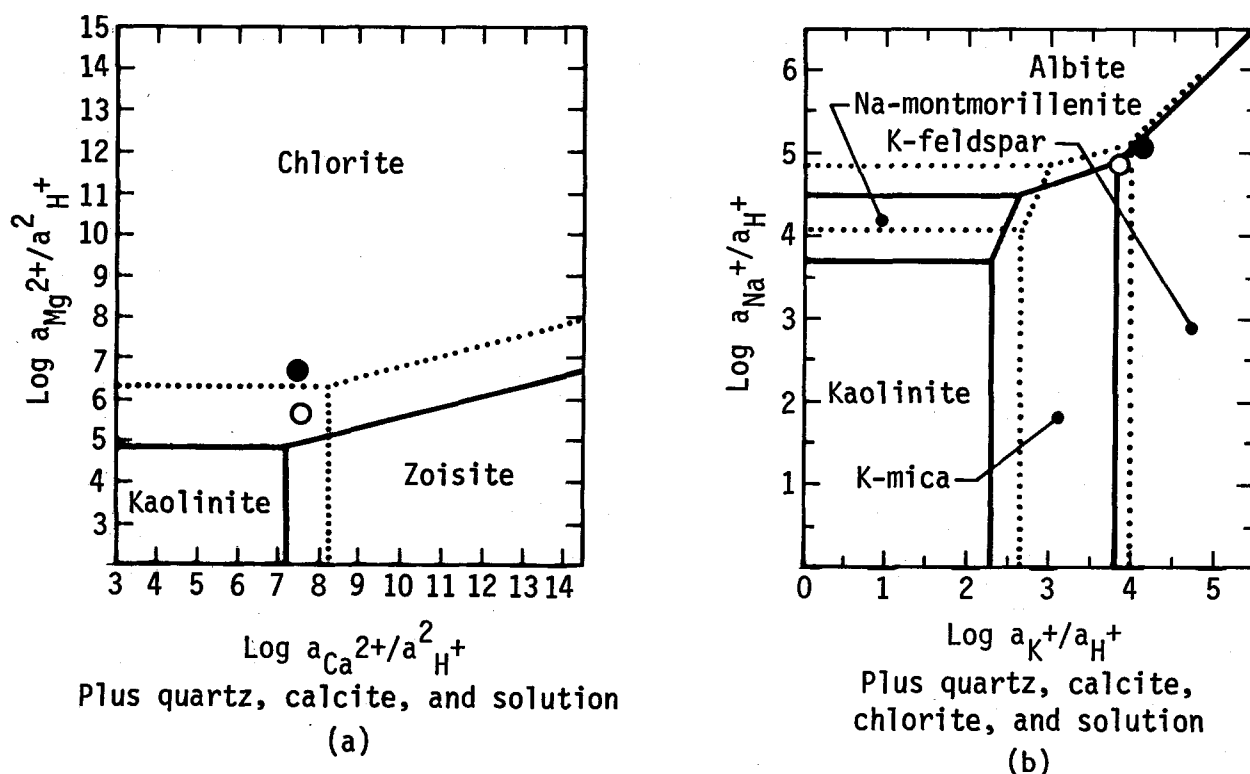


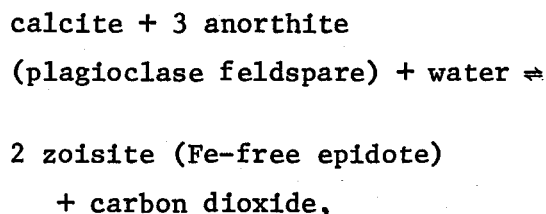
Fig. 13. Activity diagrams showing phase relations in the Salton Sea geothermal system at 250°C (dotted lines) and 300°C (solid lines). Open and solid circles depict brine chemistry from Magmamax 1 and Sinclair 4, respectively.

fall within the stability field of zoisite (epidote), thereby predicting the absence of that mineral at the two sites assuming chemical equilibrium has been attained. The usefulness of activity diagrams is apparent: they predict the mineralogy of the rock at depth in the geothermal field on the basis of temperature and brine chemistry. A detailed explanation of the theory and construction of activity diagrams is given in Appendix 1, and further comparison of the Magmamax 1 and Sinclair 4 wells will be given in a later section.

The deltaic sediments that constitute the reservoir rocks in the Salton Sea geothermal field can be described chemically by means of the complex system $\text{K}_2\text{O} - \text{CaO} - \text{Al}_2\text{O}_3 - \text{MgO} - \text{FeO} - \text{SiO}_2 - \text{CO}_2 - \text{H}_2\text{O}$, and commonly, Na_2O , Fe_2O_3 , and S. In developing a model to assess the observed mineral assemblages as well as those that might be expected at greater depths in the field, it becomes necessary to reduce the complex system to a simpler subsystem that has been studied in some detail, namely, $\text{CaO} - \text{Al}_2\text{O}_3 - \text{SiO}_2 - \text{CO}_2 - \text{H}_2\text{O}$.

Figure 14b, which has been compiled from the work of Storre and Nitsch,²² shows the isobaric phase relations at 2 kbar in the subsystem as a function of temperature and mole fraction of CO₂. The Al₂O₃ - CaO - SiO₂ composition triangle (Fig. 14a) depicts the mineral phases in the subsystem. In the T-X_{CO₂} plot, the calcite-anorthite-quartz (CAQ) triangle is adequate to describe the phase relations. The shaded arrow represents a possible reaction path with increasing depth for the Salton Sea geothermal field.

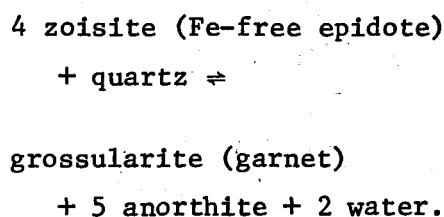
It has been recognized in this study as well as in previous ones¹³ that calcite is a principal component of unaltered reservoir rocks and epidote is common in altered rocks. Moreover, the gradual disappearance of calcite with depth coincides with the development of epidote as an alteration product. The CO₂-evolving reaction,



is a plausible means of accounting for the mineralogical observations as well as the presence of abundant CO₂ at shallow depths in the geothermal field. The slope of the univariant line representing this reaction in Fig. 14b is near infinity,

thereby making the sign of dT/dX_{CO_2} difficult to determine experimentally. Various theoretical means of estimating the sign of dT/dX_{CO_2} have led to ambiguous results, thus the univariant line is drawn vertically in Fig. 14b. If dT/dX_{CO_2} is positive, it is clear that the transition from calcite to zoisite (epidote) will occur with increasing temperature. It has been shown that the phase relations depicted in Fig. 14b will occur at lower temperatures if the pressure is reduced; for example, the invariant point labeled X is at approximately 440°C at 1 kbar.²³ Therefore, if the sign of dT/dX_{CO_2} is negative, the calcite-zoisite transition will be largely a pressure-dependent phenomenon. It is emphasized that whether the sign of dT/dX_{CO_2} is positive or negative, a mechanism exists for the calcite-epidote transition to occur with increasing depth.

Grossularite-andradite garnet has been found in cuttings from the deepest wells in the Salton Sea field,²⁴ and so it is reasonable to extend the reaction path in Fig. 14b into the garnet field by meaning of the reaction



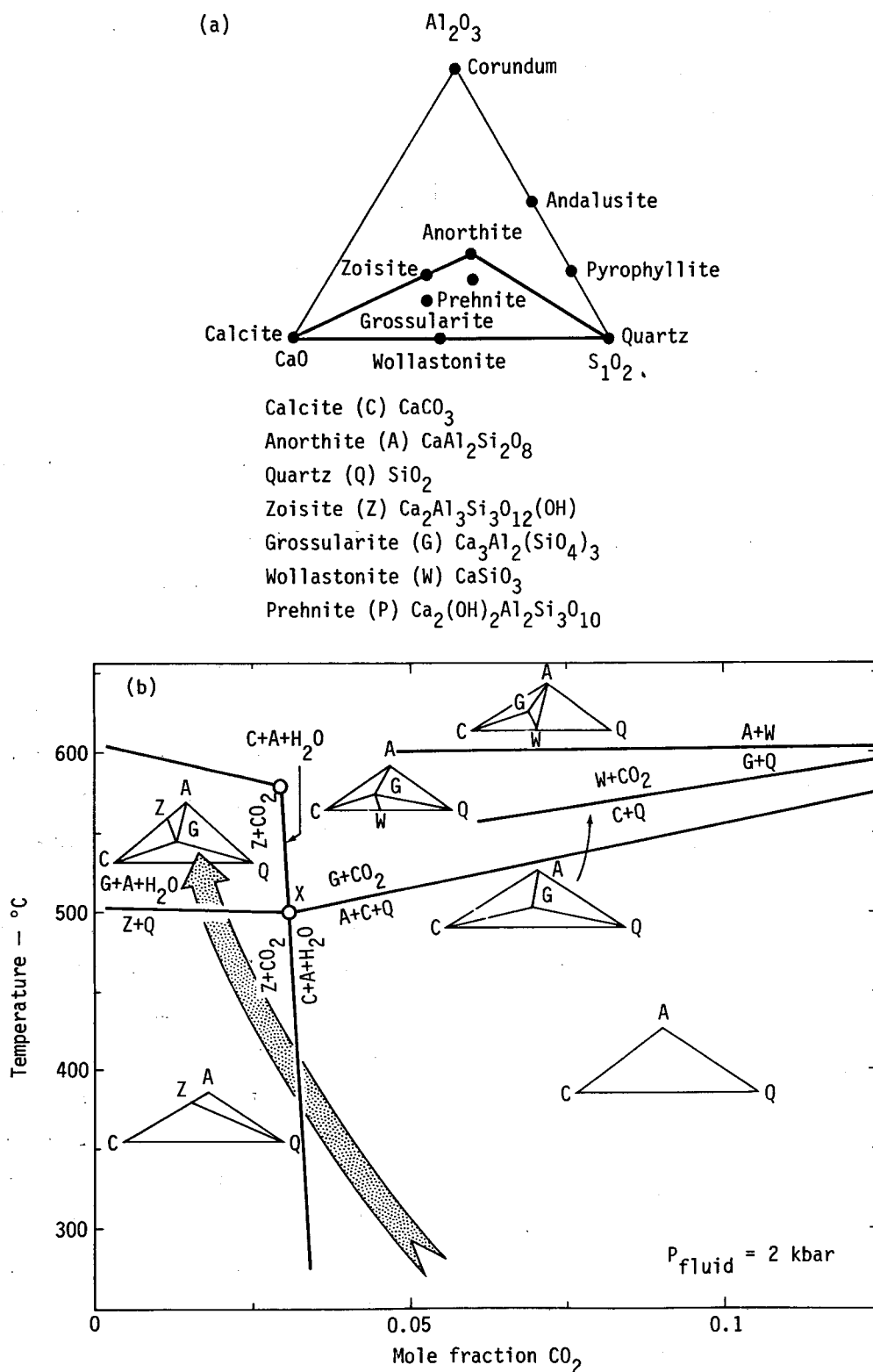


Fig. 14. The $\text{CaO}-\text{Al}_2\text{O}_3-\text{SiO}_2-\text{H}_2\text{O}$ system. (a) Mineral compositions. The calcite-anorthite-quartz (CAQ) triangle is used to depict phase relations on the $T-X_{\text{CO}_2}$ plot. (b) Temperature-mole fraction CO_2 plot at $P_{\text{fluid}} = 2 \text{ kbar}$.

The shaded arrow represents a possible reaction path for the Salton Sea geothermal field that is consistent with observations. The $T-X_{\text{CO}_2}$ plot is modified from Winkler.²²

According to the T-X_{CO₂} plot, woolastonite is another phase that might be expected at greater depths. However, pressures of 2 kbar are realized only near the bottom of the 20,000 ft (6 km) sequence of sediments in the Salton Trough. The pressures in the deepest drillholes in the Salton Sea field (8100 ft) are less than 1 kbar.

CHARACTERISTICS OF HYDROTHERMALLY ALTERED RESERVOIR ROCKS

The transition from unaltered to altered rocks in the Salton Sea field is usually rather subtle. X-ray diffraction analysis, geophysical logging, and petrographic analysis have been used by various workers to detect the onset of alteration in reservoir rocks. X-ray diffraction techniques are the most sensitive indicators of alteration and the only means by which the onset of clay mineralization can be detected. However, clay mineral transformations do not appear to have a profound effect on the petrophysical properties of reservoir rocks; therefore, a transition based on these reactions is more of academic than practical interest. Geophysical logging has been used to detect the depth at which alteration begins to effect the petrophysical properties of the rock,⁵ but this technique suffers from the

fact that it can not decipher the mineralogical characteristics of the alteration scheme. In this study, the nature of the transition was determined by petrographic analysis. Both the chemical (mineralogical) and physical changes that result from alteration can be detected by this method.

The extent and configuration of the zone of altered rocks as determined by electric log interpretation⁵ is shown in Fig. 15a. The transition to altered rocks in each well was chosen on the basis of shaly rocks acquiring carbonate-like characteristics on the electric log, i.e., high resistivity accompanied by low permeability. It is interesting to note that the first appearance of epidote in the Magmamax and Woolsey wells as determined from cutting samples in this study corresponds quite closely to Randall's picks for the top of the alteration zone in the same wells - 2660 ft (811 m) vs Randall's 2680 ft (817 m) for Magmamax 2, 2710 ft (826 m) vs Randall's 2700 ft (823 m) for Magmamax 3, and 3300 ft (1006 m) vs Randall's 3400 ft (1036 m) for Woolsey 1. Some data on the first appearance of epidote in other wells is available from Muffler and White.¹³ In IID No. 1, epidote occurs at 3450 ft (1052 m) and in Sportsman No. 1 at 3830 ft (1167 m). Although the data base is quite

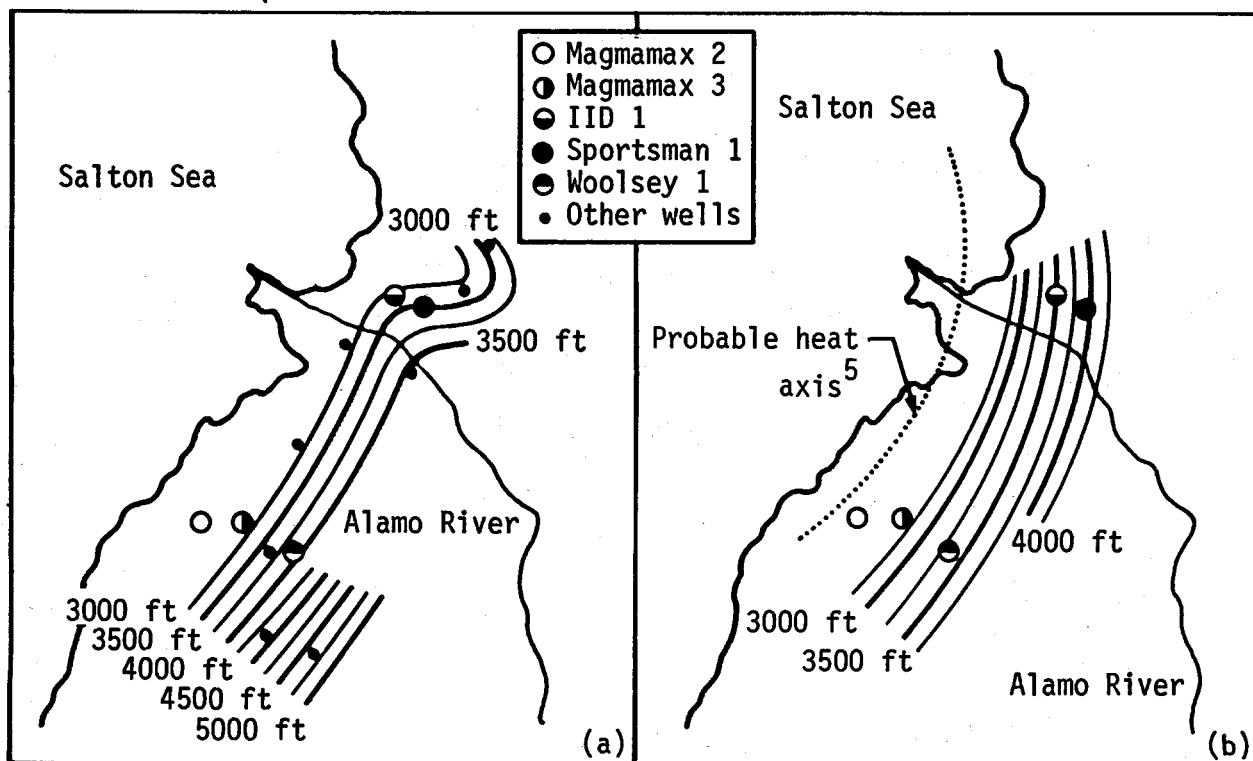


Fig. 15. Alteration zone contours. (a) The top of the metamorphic zone in the Salton Sea geothermal field as determined by electric logs.⁵ Contours are drawn on the basis of logs from 13 wells. (b) The top of the zone of alteration as determined in this study by the first appearance of epidote in drill cuttings. Contours modified from Randall⁵ on the basis of data from five wells: Magmamax 2 and 3, Woolsey 1 (this study), IID 1, and Sportsman 1.

scanty, it is worth noting that the contours of the epidote isograd i.e., the first appearance of epidote, are concentric with the probable heat axis as defined by Randall⁵ and the pattern of subsurface isotherms as determined by Palmer.²⁵

In thin section, the most obvious effect of hydrothermal alteration in sandstones and siltstones is the replacement of interstitial calcite cement with epidote and, to a lesser extent, silica. The photomicrographs

in Fig. 16 represent sandstones from the bottom (TD) of Magmamax 2 (4340 ft). Note that the grain size, texture, and mineralogy of the detrital grains (quartz, feldspar, chlorite, biotite, and lithic fragments) are very similar to those of the unaltered sandstones in Fig. 10. The sample in Fig. 16a is cemented with coarse-grained epidote, whereas in Fig. 16b the interstitial material is composed of a fine-grained intergrowth of epidote and silica. Other

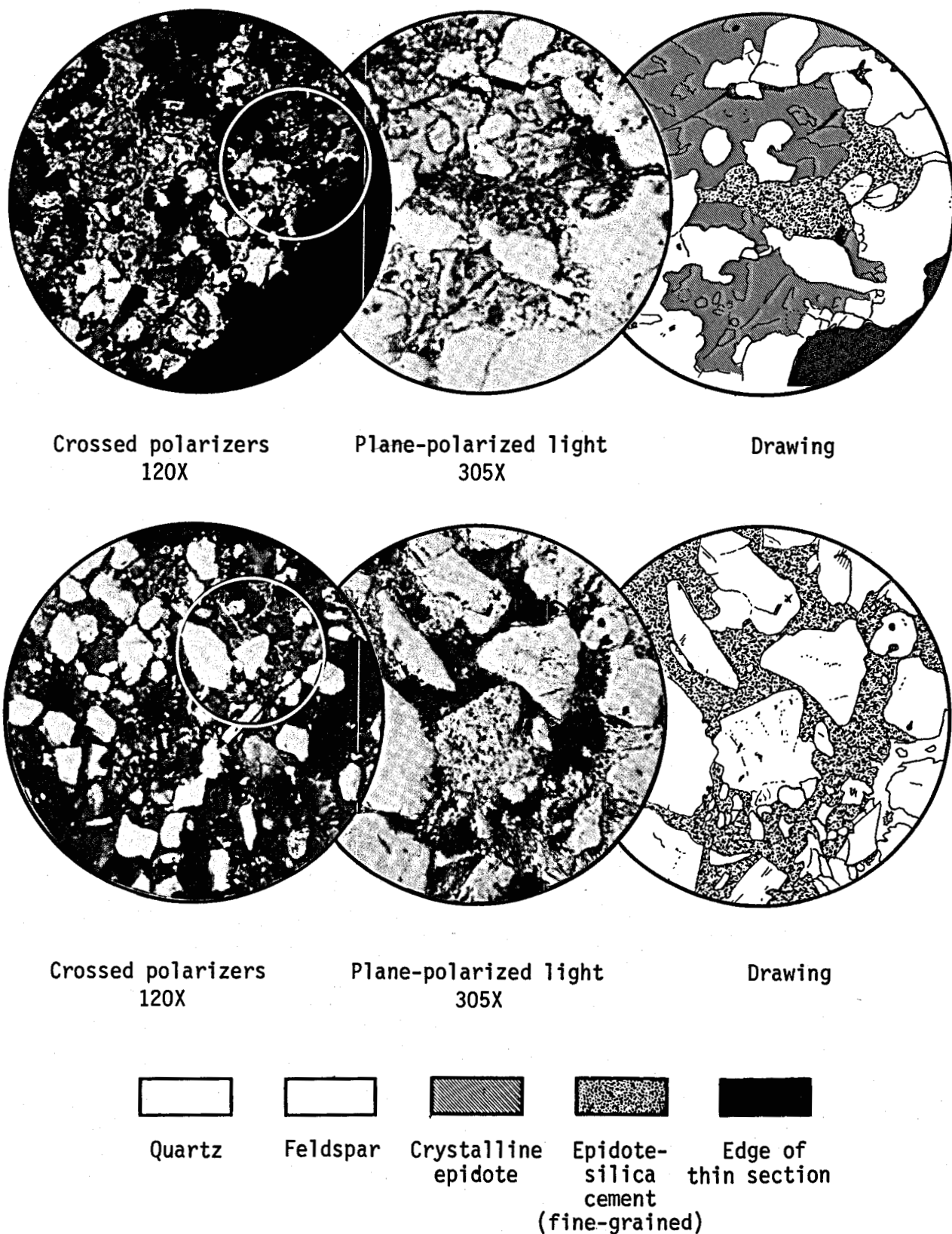


Fig. 16. Hydrothermally altered sandstones from the 4340-ft (1323-m) level (TD) in Magmamax 2. Circled areas in the 120 \times photomicrographs delimit the field of view in the 305 \times photomicrographs. The scale bar adjacent to drawings = 0.05 mm.

common pore-filling minerals in altered sandstones are pyrite, sphalerite, and hematite.

In thin section, altered shales look very much the same as the unaltered variety. In samples from below 3500 ft (1050 m) in the Magmamax wells, diffuse, fine-grained clots of epidote occur in some shaly rocks. Filled and unfilled fractures are common in shales; more will be said about this in a later section. Macroscopically, all altered rocks tend to be greenish gray in color, whereas unaltered rocks are brown, red, white, black, or gray.

Electron microprobe analyses were made of chlorite, biotite, and epidote in an altered sandstone from 4340 ft (1323 m) in Magmamax 2. The analyses were made with an eight-channel Applied Research Laboratories microprobe^{*} operated at a 15-kV accelerating potential, a 0.5- μ A beam current, and a minimum beam size. The method of Bence and Albee²⁶ and the matrix correction factors from Albee and Ray²⁷ were used to reduce the raw data. Natural silicate minerals were used as standards.

* Reference to a company or product name does not imply approval or recommendation of the product by the University of California or the U.S. Energy Research & Development Administration to the exclusion of others that may be suitable.

The complete analytical results are presented in Appendix B. The results of chlorite and biotite analyses are presented graphically on an AFKM (aluminum-iron-potassium-magnesium) projection in Fig. 17, and the results of detailed epidote analyses are presented in Fig. 18. Thin section photomicrographs of the epidote grains from the 4340-ft level of Magmamax 2 are shown in Fig. 19.

Petrographic analysis indicates that two types of chlorite are present in altered reservoir rocks; (1) very fine grained hydrothermal chlorite that is the product of clay mineral reactions and (2) coarse-grained chlorite of detrital origin. The latter type is prominent in all sandstones and siltstones, altered and unaltered. Detrital chlorite grains can be expected to have widely differing chemical compositions and yet five out of six grains analyzed from the Magmamax 2 sample fall into a fairly small composition field (Fig. 17). This suggests that the coarse-grained detrital chlorite particles in the altered sample have equilibrated with the coexisting brine. Coarse-grained detrital biotite is also found in all reservoir rocks and there is no reason a priori to believe that it is of hydrothermal origin as has been reported in previous studies. The microprobe analyses of nine biotite grains from

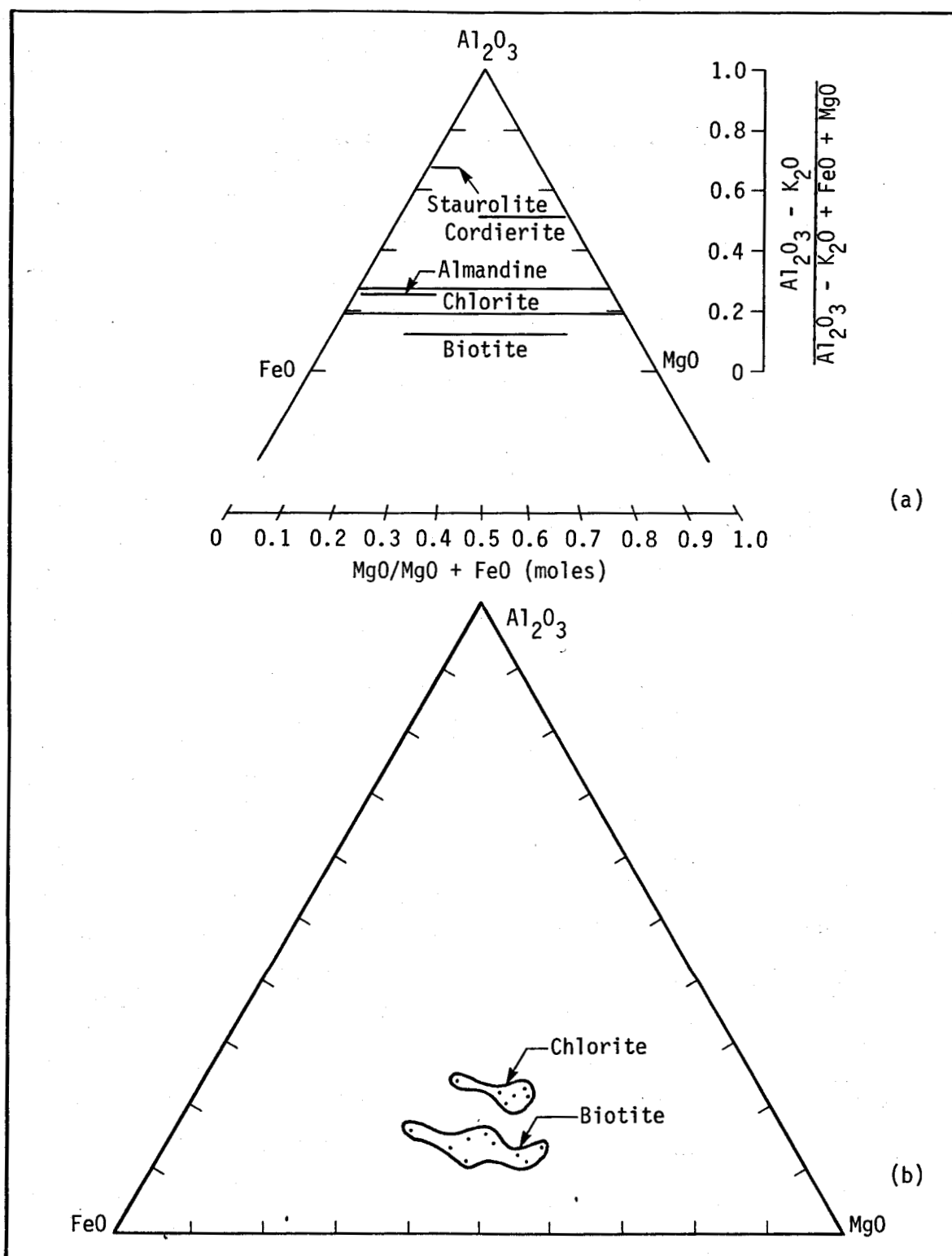


Fig. 17. Mineral compositions. (a) Compositions plotted on the projection plane of an AFKM (Thompson) projection. The range of compositions for common minerals are indicated by lines or fields. (b) Range of chlorite and biotite compositions in a single sample from the 4340-ft (1323-m) level (TD) in Magmamax 2. Total assemblage is quartz-potassium feldspar-epidote-biotite-chlorite-pyrite-hemitite.

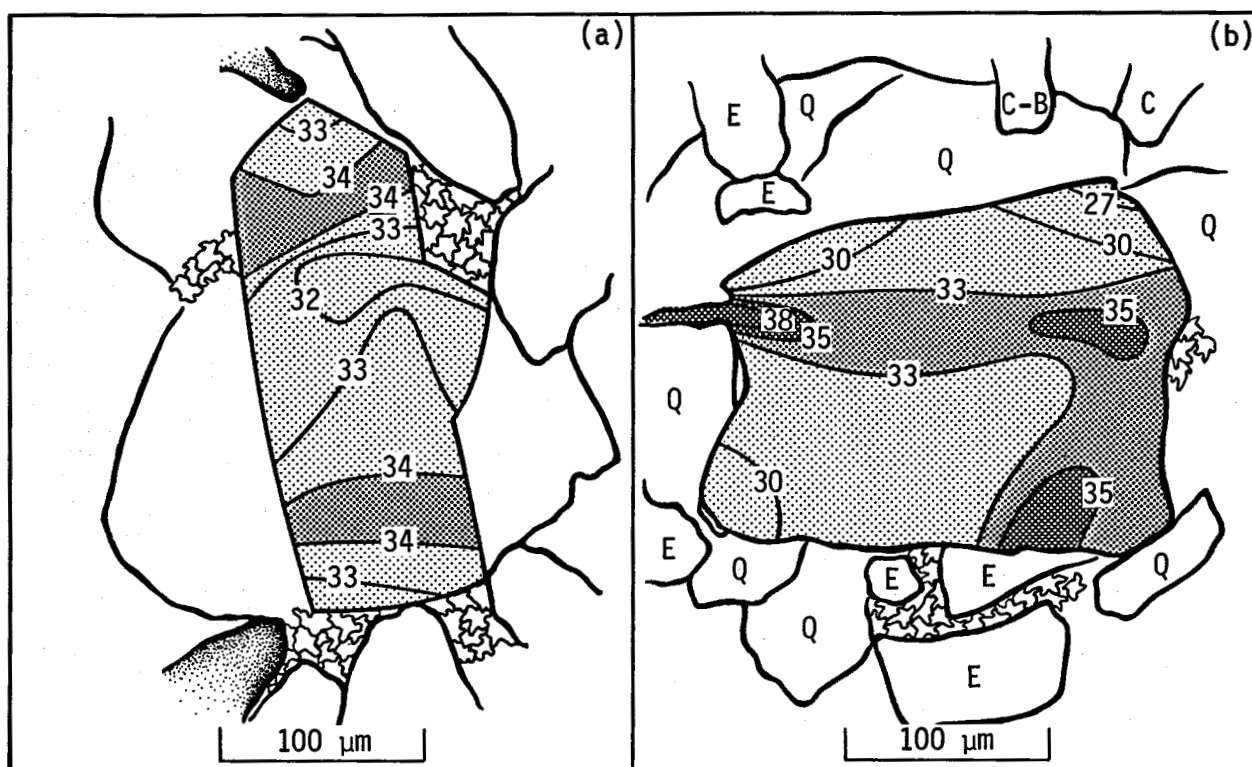


Fig. 18. Results of microprobe analysis of zoned epidote grains from the 4340-ft (1323-m) level in Magmamax 2. Contours represent the mole percent of the pistacite end-member, $\text{Ca}_2\text{Fe}_3\text{Si}_3\text{O}_{12}(\text{OH})$. Note: ideal epidote composition is $\text{Ca}_2\text{Al}_2\text{FeSi}_3\text{O}_{12}(\text{OH})$.

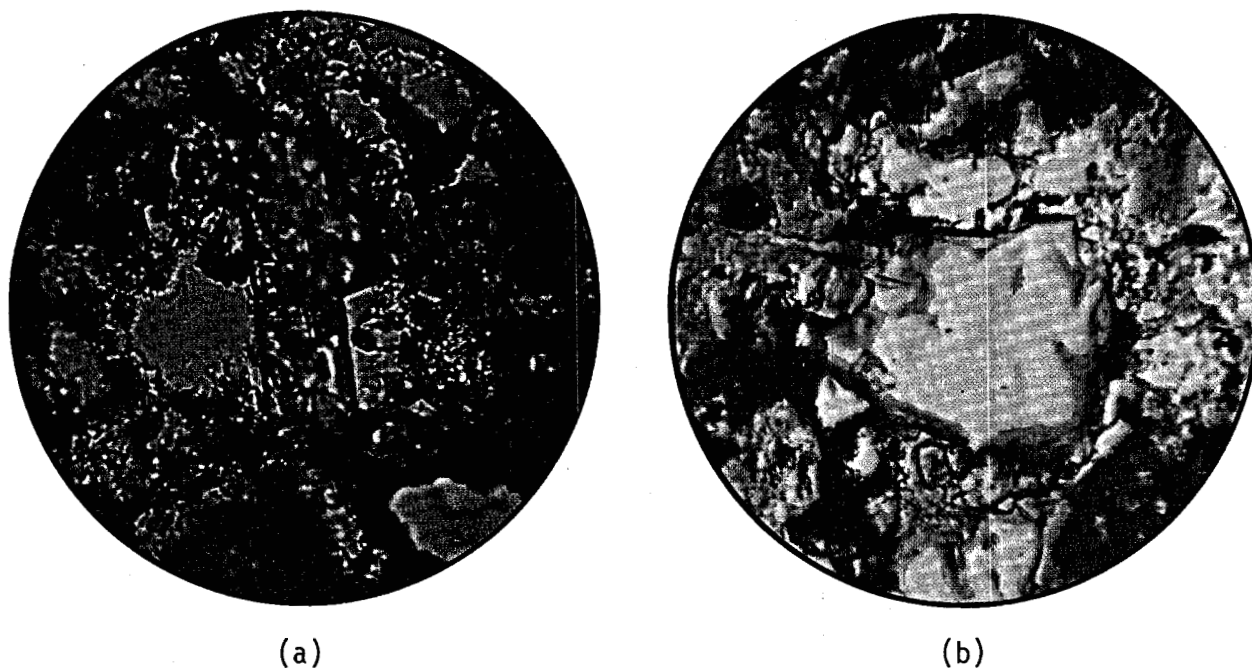


Fig. 19. Thin section photomicrographs of epidote grains in a sample from 4340-ft (1323-m) level (TD) in Magmamax 2. Magnification, 170 \times . Detailed compositions of these grains as determined from microprobe analysis are shown in Fig. 18.

a single sample (Fig. 17) exhibit a wide variety of Fe/Mg ratios and Ti values (see Appendix B), supporting the view that they are of detrital origin and suggesting that they equilibrate with brine at 300°C much less readily than does chlorite.

Detailed microprobe analysis of two epidote grains has enabled compositional contours to be drawn in terms of the mole percent of the pistacite (Ps) end-member ($\text{Ca}_2\text{Fe}_3\text{Si}_3\text{O}_{12}$). The epidotes exhibit significant zoning (Ps 27 to Ps 38) but the pattern is not a regular one. One notable feature is that the Ps content tends to be low in the "corners" and along edges. Nucleation of hydrothermal mineral grains tends to occur along the edges of voids (see Fig. 20) and therefore the growth pattern can be interpreted as one that began in the "corners" and proceeded inward toward the middle of the void. The composition of epidote is reported to be a strong function of the oxygen fugacity level present in the rock during the process of hydrothermal alteration.²⁸ As the $f\text{O}_2$ level increases the Ps component in epidote increases concomitantly. Therefore, it appears that the epidotes in Fig. 19 grew under conditions of increasing oxygen fugacity levels, i.e., the brine became more oxidizing during on-going alteration.

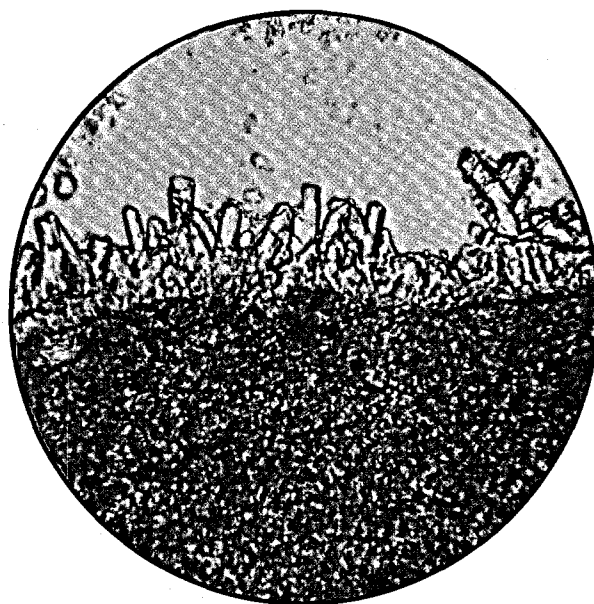


Fig. 20. Well-formed epidote crystals in partially filled fracture in shale. The sample is from the 2750-ft (840-m) level in Magmamax 2. Magnification, 370×, plane-polarized light.

THE EFFECTS OF ALTERATION ON RESERVOIR PROPERTIES

The obvious effect of hydrothermal alteration on the reservoir rocks in the Salton Sea geothermal field has been the reduction of porosity and permeability. Epidote and silica are the principal pore-filling minerals produced during high-temperature alteration. They replace calcite and anhydrite, the cementing agents produced during diagenesis (Fig. 21). Facca and Tonani¹¹ introduced the concept of the self-sealing geothermal field that was discussed earlier. Their concept is a simple one: hot brine infiltrates permeable



Fig. 21. Large fracture in shale completely filled with anhydrite. The sample is from the 3630-ft (1110-m) level in Magmamax 2. Magnification, 52 \times , crossed polarizers.

rock and deposits minerals in the pore space, thereby decreasing the porosity and permeability. The process is beneficial when it serves to create an impermeable cap rock over a shallow geothermal reservoir. It is detrimental when it reduces porosity and permeability in reservoir rocks.

Porosity measurements were made on core samples from two intervals in Woolsey No. 1 and three intervals in State of California No. 1. The results are plotted in Fig. 22, and a detailed listing of the data is provided in Appendix C. The plotted results indicate a reduction in porosity with depth. This is a com-

mon characteristic of sedimentary basins and is likely to be enhanced in the Salton Sea geothermal field by hydrothermal alteration effects.

It is expected that the magnitude of vertical porosity gradients would vary with respect to location within the geothermal field, becoming steeper toward the center. It should be noted that Woolsey No. 1 and State of California No. 1 are approximately equidistant from the heat axis of the field.⁵ Therefore, the data plotted in Fig. 22 are likely to be compatible in that the two wells represent areas with porosity gradients of similar magnitude.

In the area studied, geophysical log and drill core data indicate that the reservoir strata dip westward toward the center of the geothermal resource at a 5 to 10° angle (Fig. 23). In the presence of a vertical porosity gradient, the dipping strata become progressively deeper and concomitantly less porous and permeable in going from the periphery of the field in toward the center of the heat axis. Measured porosities of unaltered sandstone core samples from the 2570-ft (783-m) level in Woolsey No. 1 are over 20% (Fig. 22), and porosities of over 30% have been estimated for drill cutting chips from the same interval. Log correction shows that this same sandstone sequence occurs at the 3050-ft

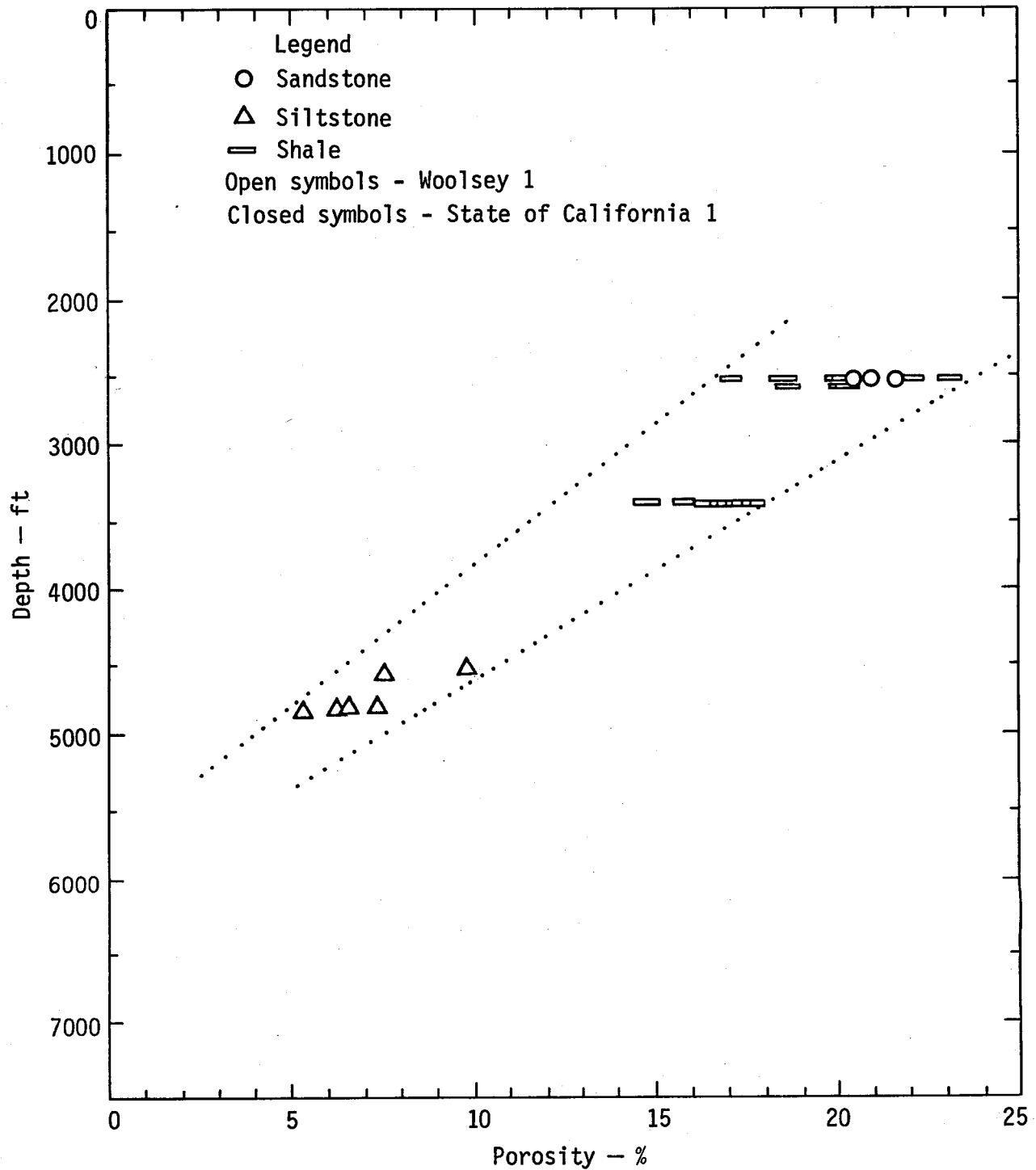


Fig. 22. Plot of porosity vs depth for cores from Woolsey 1 and State of California 1 wells. Note the sharp decrease in porosity with depth.

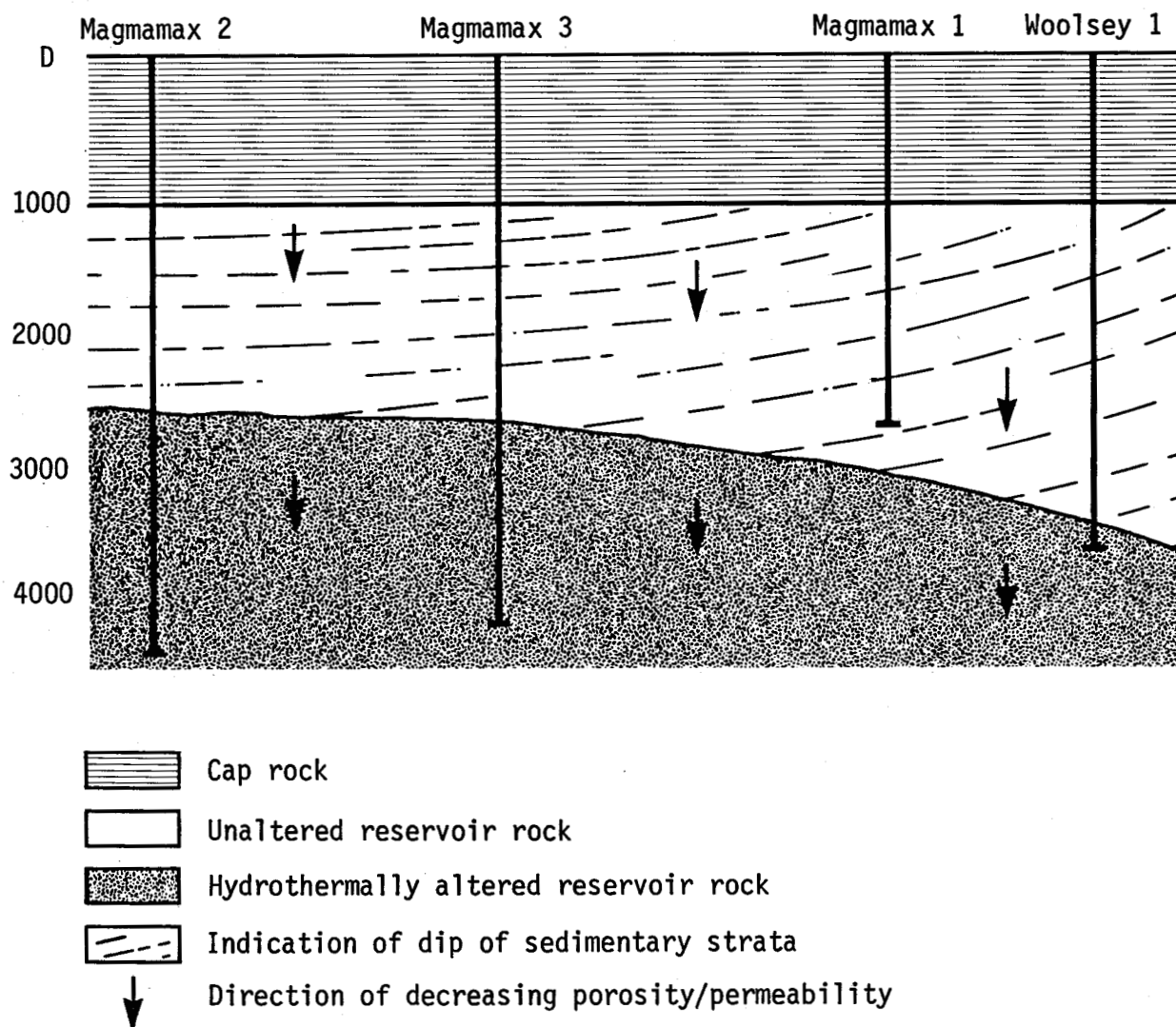


Fig. 23. East-west cross section through the Magmamax and Woolsey wells depicting directional mode of porosity gradients. The three rock types — cap rock, unaltered reservoir rocks, and hydrothermally altered rocks — are my classifications based on petrographic analysis. Boundaries between rock types are those determined in this report.

(930-m) level in Magmamax 2 and, therefore, is within the zone of hydrothermal alteration. The pore space has been well filled with epidote and the porosity is estimated to be less than 10%.

Admittedly, the hypotheses concerning porosity gradients in the

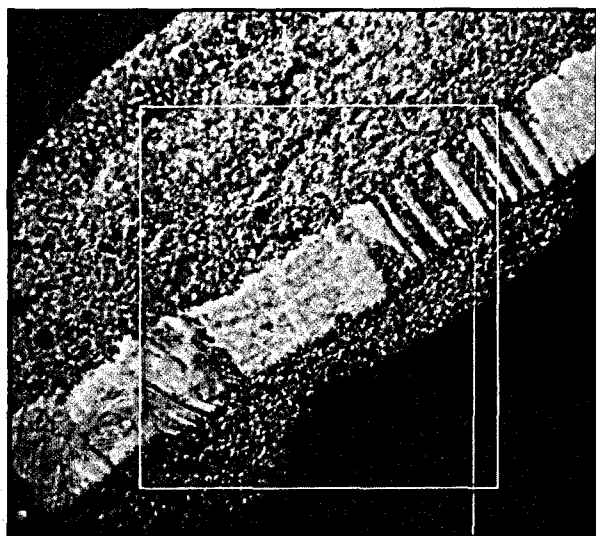
geothermal field are based on data from a small number of wells. Since a knowledge of porosity/permeability gradients is of importance in planning for future production of the resource, an effort should and will be made to corroborate the hypotheses with data from other wells.

THE SIGNIFICANCE OF FRACTURE POROSITY AND PERMEABILITY

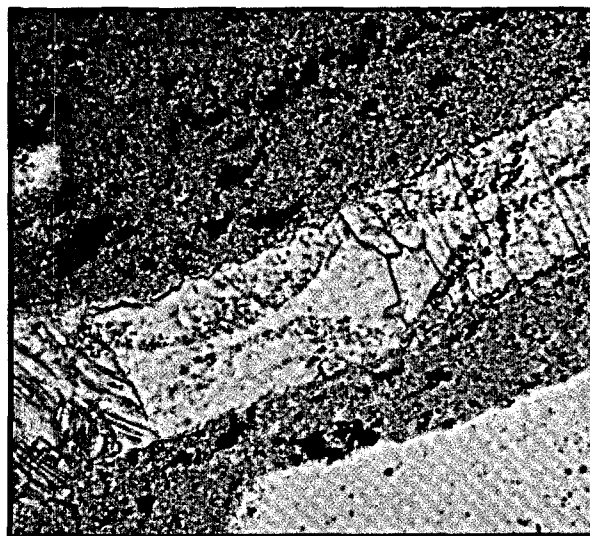
It is noteworthy that fractures provide a substantial portion of the permeability and reservoir capacity in a number of geothermal fields, e.g., Geysers, Otake, Larderello, Wairakai, and Broadlands.²⁹ While the primary intergranular porosity in a reservoir is subject to irreversible self-sealing, fractures can be considered as "renewable" porosity and/or permeability because they can be reactivated subsequent to being filled or sealed. The fracture-producing mechanism may be either natural seismicity (many geothermal fields are located in tectonically

active areas) or natural hydraulic fracturing resulting from high fluid pressures in the reservoir.³⁰

The reservoir rocks in the Salton Sea geothermal field are extensively fractured, especially the shales. Fracture widths range from a few micrometres to 1 cm. The nature of cutting samples did not permit me to estimate fracture length or surface area. Most of the observed fractures in 4-in.-diam core samples from State of California No. 1 and 3-in.-diam cores from Woolsey No. 1 extend beyond the sample boundaries and exhibit offset. The location of the Salton Sea field on an active spreading zone⁴ ostensibly can account for the myriad fractures in the reservoir.

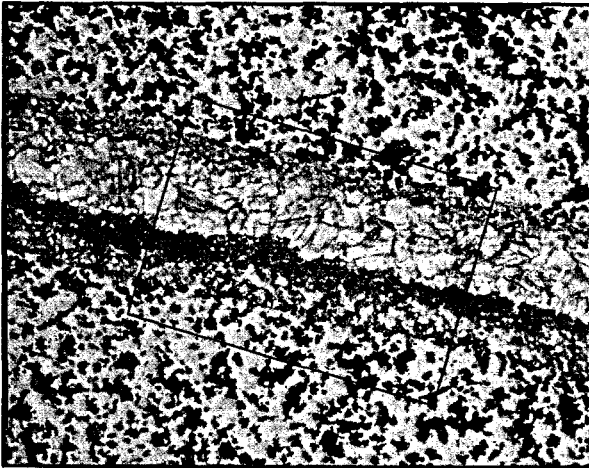


(a) Crossed polarizers

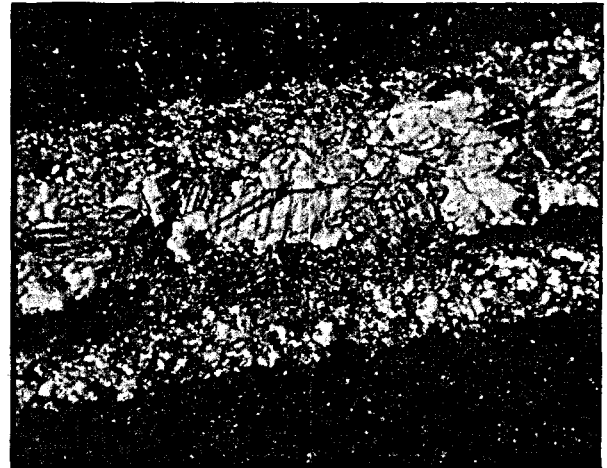


(b) Plane polarized light

Fig. 24. Calcite vein in shale from the 3630-ft (1110-m) level in Magmamax 2. The calcite has been mechanically twinned subsequent to deposition, indicating renewed stress along an old fracture. Area outlined in (a) represents the field of view in (b).



(a) Plane polarized light



(b) Crossed polarizers

Fig. 25. Calcite-epidote vein in shale from the 3820-ft (1167-m) level in Magmamax 3. The composite vein is interpreted as originally being a calcite-filled fracture that was subsequently refractured with epidote filling the second fracture. Area outline in (a) represents the field of view in (b).

Evidence for the "renewability" of fracture porosity/permeability subsequent to sealing is exhibited in Figs. 24 and 25. In Fig. 24 the calcite in a sealed fracture has been mechanically twinned and deformed subsequent to deposition, indicating that there has been renewed stress on the old fracture. Figure 25 is interpreted as representing a calcite-filled fracture that has been reactivated (refractured) and subsequently

refilled with epidote. Observations of cathodoluminescence of calcite vein fillings reveals two or more episodes of calcite deposition in many samples. This further corroborates the "renewability" of fractures. In drill cutting samples, open fractures manifest themselves as planar surfaces coated with a thin layer of a fracture-filling mineral. Such samples are common in the cuttings from Magmamax Nos. 2 and 3.

Well Log Correlation

Spontaneous potential (SP), resistivity, and temperature logs have been commonly run in the Salton Sea

geothermal wells subsequent to drilling and prior to setting liners. Spontaneous potential (SP) logs give

qualitative indications of the relative sandiness/shaliness of sedimentary strata and provide good indications of stratigraphic boundaries. As such they are useful for correlation purposes and have been so utilized in this study (Figs. 26 to 28).

Spontaneous potential log correlations for the Magmamax and Woolsey wells are given in Fig. 26. The use of shading and dotted connecting lines is intended to help the reader visualize the correlations proposed here. The sequence of regularly alternating sand and shale beds overlying a major shale break in the vicinity of 2000 ft (625 m) in Woolsey 1, 2250 ft (700 m) in Magmamax 1, and 2500 ft (775 m) in Magmamax 2 and 3 is the most readily correlatable interval in the section and is, therefore, useful in establishing the correlation pattern among the four wells. With the pattern established, it has been possible to make other unambiguous correlations above and below the key interval. The geologic picture that emerges from the proposed correlations is that of a structural basin whose axis or center lies to the northwest of Magmamax 2. The picture is compatible with the cross section of the Salton Trough in Fig. 2, and the magnitude of the dip of the strata correlates well with the dip measured in cores taken from Woolsey No. 1. The cap

rock in the four wells produces a rather featureless SP curve and as such is readily recognizable at the top of each log. The transition between unaltered and hydrothermally altered reservoir rocks is not apparent in the SP logs.

The interval from approximately 2370 to 2650 ft (725 to 810 m) in Woolsey No. 1 has been carefully studied and is shown in diagrammatic form in Fig. 27. The most notable feature in the interval is the thick sandstone bed extending from 2450 to 2540 ft (747 to 774 m). The porosity has been estimated in thin section to be at least 30%, the highest found in cuttings from three wells. Portions of the sandstone interval from 2570 to 2585 ft (783 to 788 m) were recovered as core, and the porosity was measured in the laboratory. The average porosity of three samples was 21% (see Table C1, Appendix C). The sandstones are cemented with silica and calcite. The shales exhibit numerous fractures; some the result of soft sediment deformation (e.g., the clay-filled fracture in Fig. 27), other the result of hard-rock deformation (calcite and pyrite veins in Fig. 27)

A correlation of the SP log with the drill cuttings log is shown in Fig. 28. The problems encountered with cuttings were discussed in an earlier section. The particular

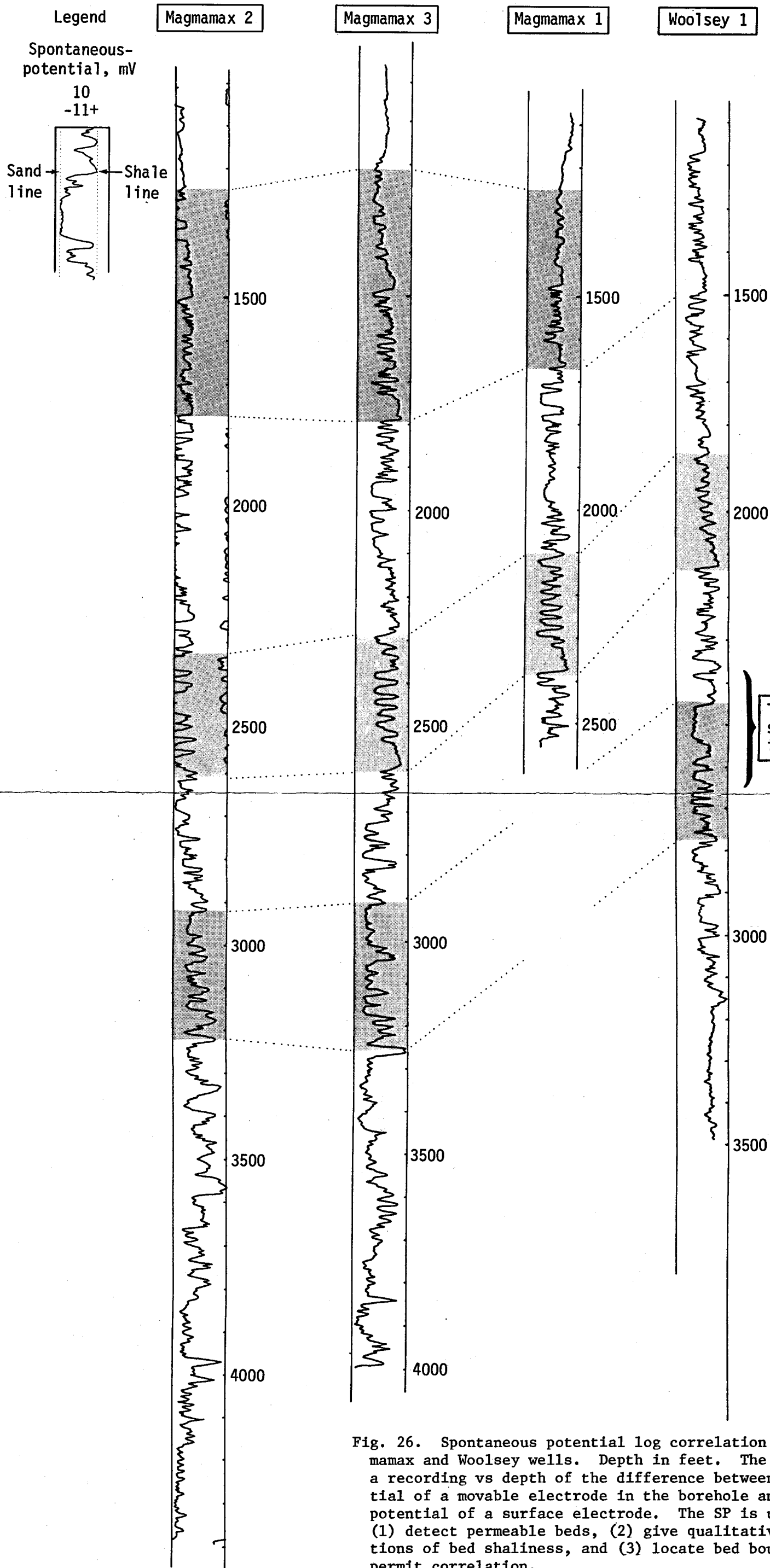


Fig. 26. Spontaneous potential log correlation of the Magmax and Woolsey wells. Depth in feet. The SP curve is a recording vs depth of the difference between the potential of a movable electrode in the borehole and the fixed potential of a surface electrode. The SP is useful to: (1) detect permeable beds, (2) give qualitative indications of bed shaliness, and (3) locate bed boundaries and permit correlation.

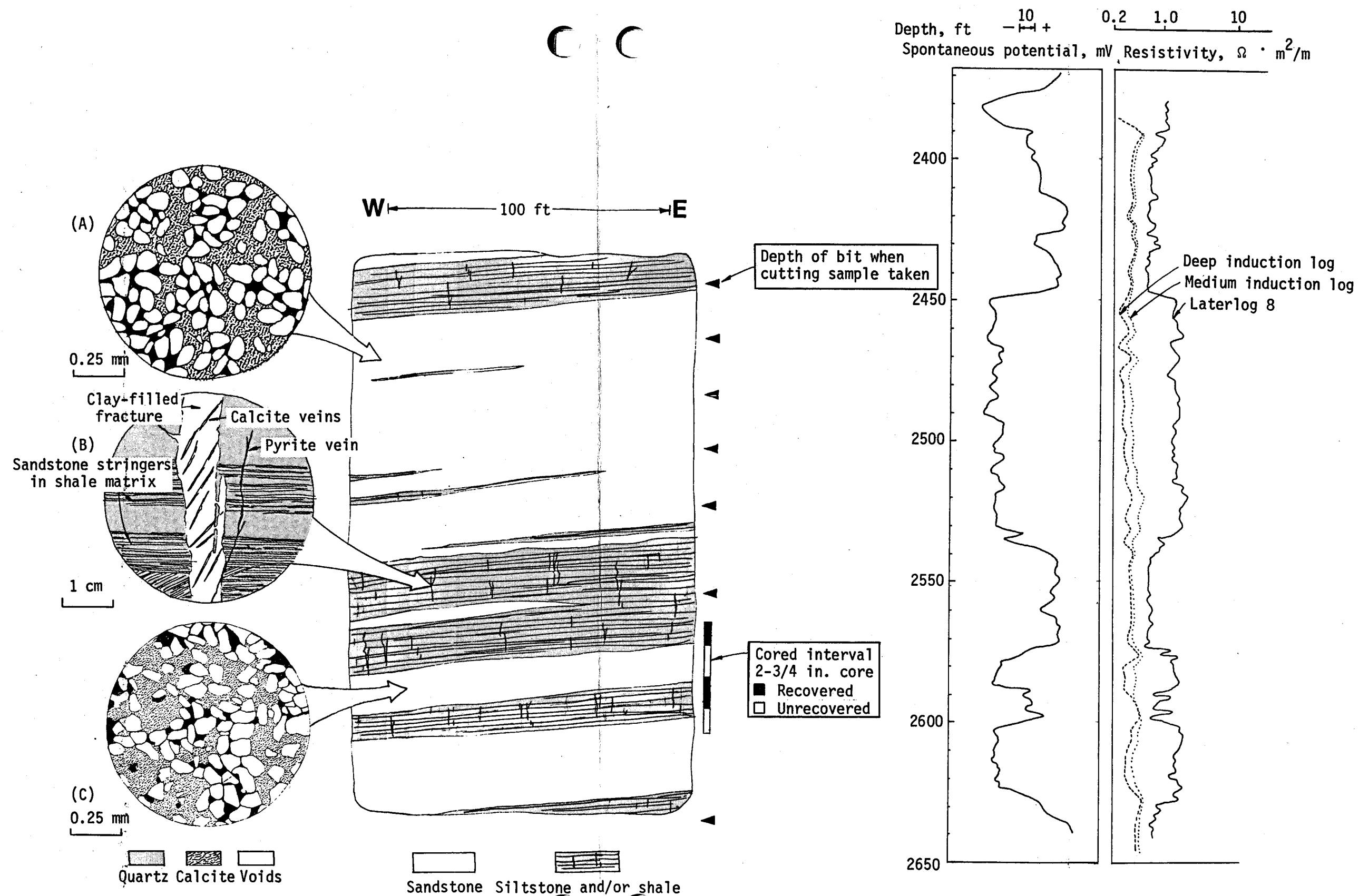
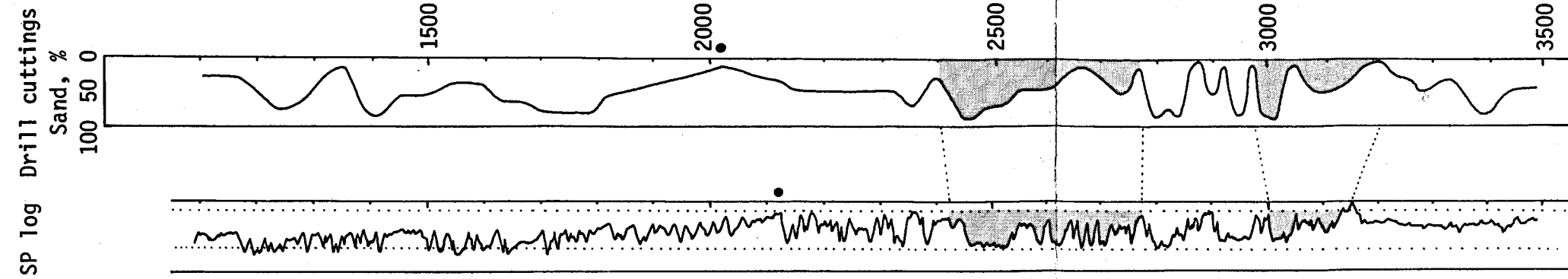
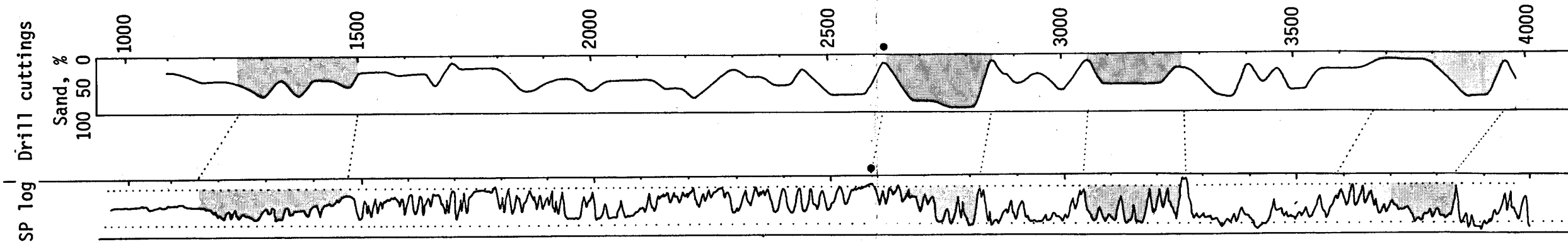


Fig. 27. Detail of electric log and corresponding lithology over the interval 2400 to 2650 ft (730 to 810 m) in Woolsey 1.

Woolsey 1



Magmamax 3



Magmamax 2

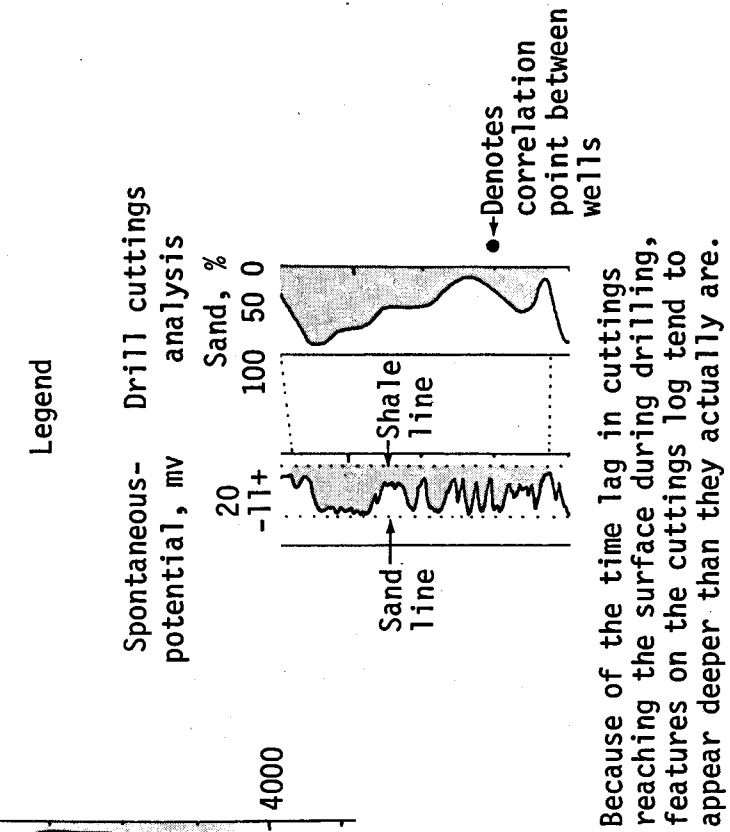
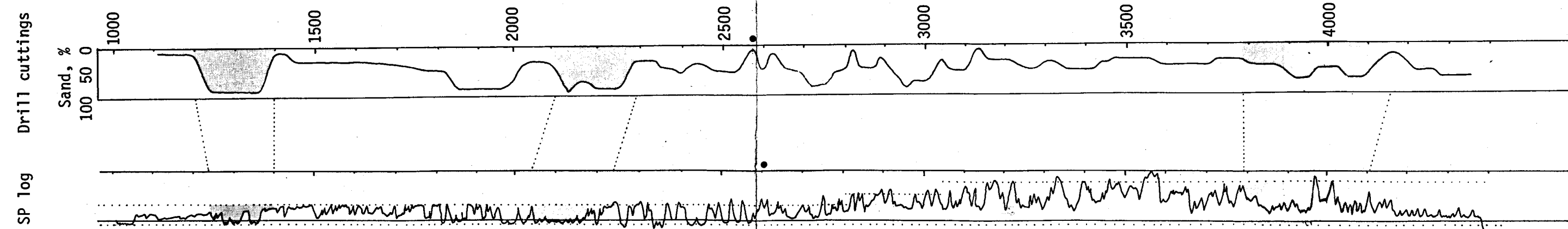


Fig. 28. Correlation of SP log and drill cuttings analysis.

problems of the "smoothing" and displacement of features is evident when the two logs are compared. The gross features of the SP log are mirrored in the cuttings analysis, but it is clear that the plotting of precise

production intervals would be difficult if based solely on the cuttings log. Again, the shaded portions of the logs are meant only to aid the reader's eye and are intended to have no other significance.

A Comparison of Two Geothermal Wells

Sinclair No. 4 and Magmamax No. 1 are two producing geothermal wells in the Salton Sea geothermal field. Sinclair 4 produces from deep reservoir rocks [4400 ft (1340 m)] whereas Magmamax 1 produces from relatively shallow rocks [1900 ft (580 m)]. It is useful and informative to compare a number of characteristics of the two production regimes.

The Sinclair 4 well was completed to a depth of 5300 ft (1615 m) in June 1964, and production characteristics at that time were 450,000 lbs/hr (20% steam) at a wellhead pressure of 250 psi and temperature of 165°C.³¹ The well has been used as production for mineral extraction operations and was reconditioned as a geothermal test facility in 1973. More recent production characteristics for similar flow rates (15% steam) are 220 psi at 210°C.³² Magmamax 1 was completed to a depth of 2805 ft (855 m) in January 1972, and the average production characteristics at that time were 410,000 lbs/hr (13% steam) at a well-

head pressure of 115 psi and temperature of 175°C.³¹ It is currently being used as the production well for the San Diego Gas and Electric Company's geothermal test facility. More recent production data for similar flow rates (10% steam) are 275 psi at 210°C.³³

The principal cross section in the block diagrams of Fig. 29 intersects Magmamax 1 and Sinclair 4. The isothermal contours in Fig. 29a have been drawn on the basis of data from Palmer.⁶ The regions in the diagram characterized by widely spaced isothermal surfaces are interpreted as being sand-rich. The basis of this interpretation is that permeable sand reservoirs permit the circulation and/or convection of brine, which serves to diminish the local thermal gradient, thereby resulting in widely spaced isotherms. For the opposite reasons, closely spaced isotherms are interpreted as shaly layers. The isotherm pattern in the vicinity of the 500-m depth suggests that a

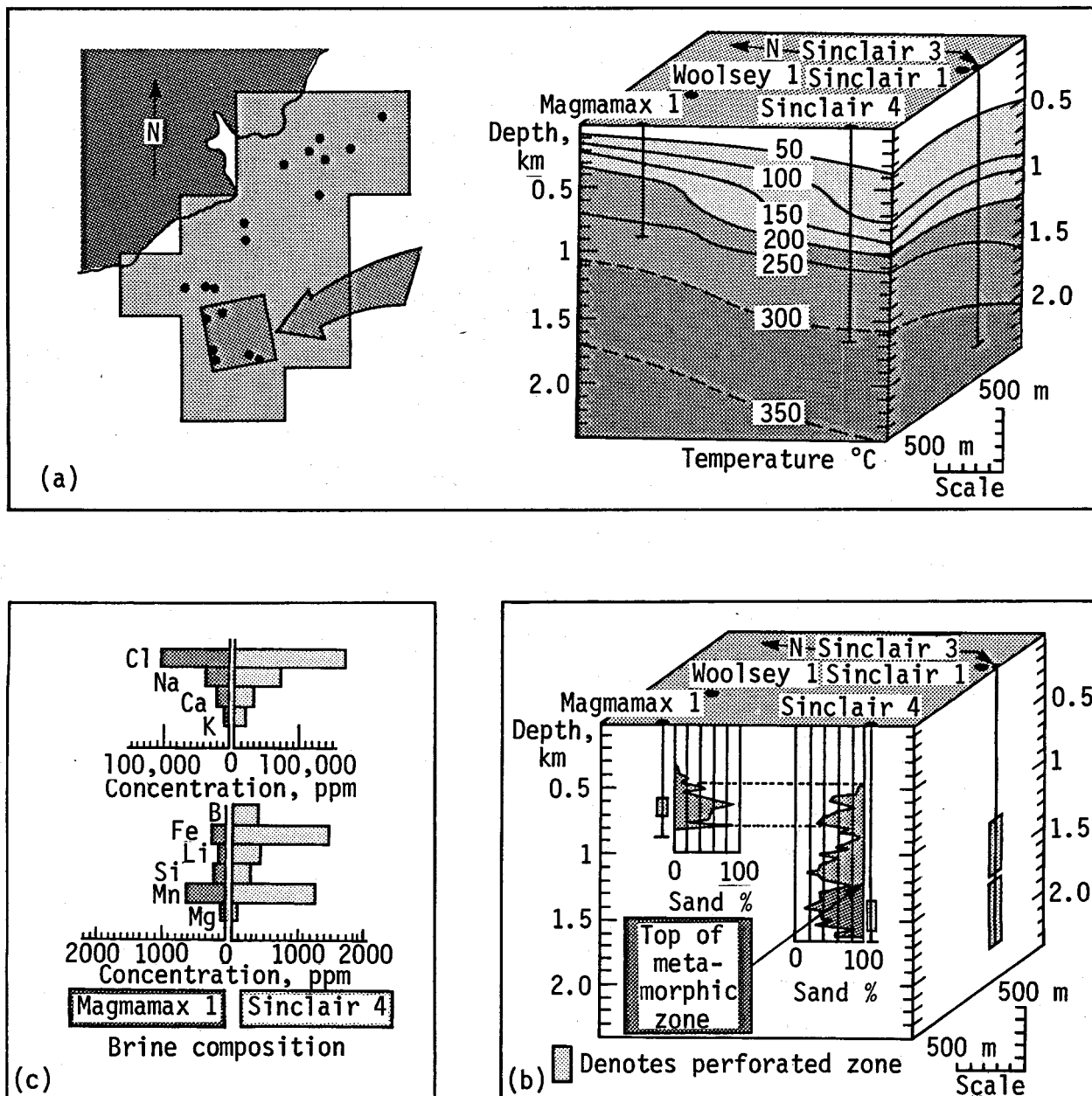


Fig. 29. Magmamax and Sinclair well comparisons. (a) Block diagram of isothermal surfaces in the vicinity of the Magmamax and Sinclair wells (see inset locator map) in the Salton Sea geothermal field. Temperature data from Palmer.⁶ (b) Comparison of reservoir characteristics in the Magmamax 1 and Sinclair 4 wells. Sand analysis and correlation between wells from Towse and Palmer,⁸ top of metamorphic zone from Randall,⁵ and data on perforated intervals from Palmer.⁶ (c) Comparison of brine composition in Magmamax 1 and Sinclair 4.

300-m-thick sandy layer extends between the two wells. This interpretation is supported by the sand analysis based on geophysical logs that is shown in Fig. 25b.⁸ The Magmamax well has been perforated in this uppermost sand sequence; the Sinclair well is perforated in deeper reservoir rocks. The permeability of the perforated zones in the two wells is likely to be quite different, because the reservoir in Sinclair 4 is within a deep zone of altered rocks according to Randall,⁵ and the Magmamax 1 reservoir is in unaltered reservoir rocks.

There is a significant difference in the brine chemistry at the two sites manifested in terms of the scaling rate during production. The brine at Magmamax 1 has total dissolved solids of 175,000 ppm,³⁴ whereas the total for Sinclair No. 4 is nearly twice as much, 300,000 ppm.³² Although the test facilities at both wells have had scaling problems, those at Sinclair 4 have been more severe because of the higher solute content of the brine. The difference in brine chemistry at the two sites can be attributed to temperature, as illustrated by Helgeson (p. 143).⁷

Acknowledgments

I gratefully acknowledge the contributions that others have made to this study. Jack Howard, formerly of Lawrence Livermore Laboratory and now at Lawrence Berkeley Laboratory, conceived the project and obtained cutting samples from the Magma Power Company wells for my use. During the writing of the manuscript, discussions with Jack Howard, Paul Kasameyer, Larry Owen and Donald Towse of Lawrence Livermore Laboratory; Patrick Browne of the New Zealand Geological

Survey; and Lori Dengler of the University of California, Berkeley, helped to clarify my thoughts on a number of important points. The manuscript was improved as a result of reviews by Howard, Kasameyer, Owen, Donald Miller, and Donald Emerson. William Beiriger, Edward Britton, and Terry Mayer provided invaluable technical assistance. The assistance of Katie Young in getting the manuscript into final form is greatly appreciated.

References

1. T. W. Dibblee, Jr., "Geology of the Imperial Valley Region, California, Pt. 2," in *Geology of Southern California*, R. H. Jahns, ed., *California Div. Mines Bull.* 170, 21-28 (1954).
2. S. Biehler, R. L. Kovach, and C. R. Allen, "Geophysical Framework of Northern End of Gulf of California Structural Province," in T. H. Van Andel, and G. G. Shor, Jr., eds., *Marine Geology of the Gulf of California - A Symposium* (Am. Assoc. Petrol. Geol. Mem. Vol. 3), (1964).
3. L. J. P. Muffler and B. R. Doe, "Composition and Mean Age of Detritus of the Colorado River Delta in the Salton Trough, Southeastern California," *Jour. Sed. Petrol.*, 38, No. 2, 384-399 (1968).
4. W. A. Elders, R. W. Rex, T. Meidav, P. T. Robinson, and S. Biehler, "Crustal Spreading in Southern California," *Science* 178, No. 4056, 15-24 (1972).
5. W. Randall, *An Analysis of the Subsurface Structure and Stratigraphy of the Salton Sea Geothermal Anomaly, Imperial Valley, California*, Ph.D. thesis, University of California, Riverside, California (1974).
6. T. D. Palmer, *Characteristics of Geothermal Wells Located in the Salton Sea Geothermal Field, Imperial County, California*, Lawrence Livermore Laboratory, Rept. UCRL-51976 (1975).
7. H. C. Helgeson, "Geologic and Thermodynamic Characteristics of the Salton Sea Geothermal System," *Am. Jour. Sci.* 266, 129-166 (1968).
8. D. F. Towse and T. D. Palmer, *Summary of Geology at the ERDA-Magma-SDG&E Geothermal Test Site*, Lawrence Livermore Laboratory, Rept. UCID-17008 (1976).
9. P. C. Van de Kamp, "Holocene Continental Sedimentation in the Salton Basin, California: A Reconnaissance," *Geol. Soc. Amer. Bull.* 84, 827-848 (1973).
10. R. A. Berner, *Principles of Chemical Sedimentology* (McGraw-Hill, New York, (1971).
11. G. Facca and F. Tonani, "The Self-Sealing Geothermal Field," *Bull. Volcanologique* 30, 271-273 (1967).
12. M. L. Batzle and G. Simmons, "Microfractures in Rocks from Two Geothermal Areas," *Earth. Plant. Sci. Letters* 30, 71-93 (1976).

13. L. J. P. Muffler and D. E. White, "Active Metamorphism of Upper Cenozoic Sediments in the Salton Sea Geothermal Field and the Salton Trough," *Geol. Soc. Amer. Bull.* 80, 157-182 (1969).
14. J. L. LeConte, "Account of Some Volcanic Springs in the Desert of the Colorado in Southern California," *Am. Jour. Sci.*, 2nd ser 19, 1-6 (1855).
15. C. Kendall, California Institute of Technology, private communication (1976).
16. D. K. Bird and W. A. Elders, "Hydrothermal Alteration and Mass Transfer in the Discharge Portion of the Dunes Geothermal System, Imperial Valley of California, USA," in *Proceedings, Second United Nations Symposium on the Development and Use of Geothermal Resources*, San Francisco, California, Vol. 1 (1976), pp. 285-295.
17. B. J. Skinner, D. E. White, H. J. Rose, and R. E. Mays, "Sulfides Associated with the Salton Sea Geothermal Brine," *Econ. Geol.* 62, 316-330 (1967).
18. L. C. Dutcher, W. F. Hardt, and W. R. Moyle, Jr., "Preliminary Appraisal of Ground Water in Storage with Reference to Geothermal Resources in the Imperial Valley Area, California," *U.S. Geological Survey Circular* 649, (1972).
19. H. C. Helgeson, "Solution Chemistry and Metamorphism," in P. H. Abelson, ed., *Researches in Geochemistry*, Vol. 2 (New York, John Wiley and Sons, 1967), p. 362-404.
20. J. J. Hemley, "Some Mineralogical Equilibria in the System $K_2O-Al_2O_3-SiO_2-H_2O$," *Am. Jour. Sci.* 257, 241-270 (1959).
21. J. J. Hemley and W. R. Jones, "Chemical Aspects of Hydrothermal Alteration with Emphasis on Hydrogen Metasomatism," *Econ. Geol.* 59, 538-569 (1964).
22. B. Storre and K. H. Nitsch, "Die Reaktion 2 Zoisite + 1 CO_2 = 3 anorthite + 1 calcite + 1 CO_2 ," *Contrib. Mineral. Petrol.* 35, 1-10 (1972).
23. H. G. F. Winkler, *Petrogenesis of Metamorphic Rocks*, (Springer-Verlag, New York, 1976), 4th Ed.
24. P. R. L. Browne, New Zealand Geological Survey, private communication (1976).
25. T. D. Palmer, J. H. Howard, and D. P. Lande, *Geothermal Development of the Salton Trough, California and Mexico*, Lawrence Livermore Laboratory, Rept. UCRL-51775 (1975).

26. A. E. Bence and A. L. Albee, "Empirical Correction Factors for the Electron Microanalysis of Silicates and Oxides," *Jour. Geology* 76, 382-403 (1968).
27. A. L. Albee and L. Ray, "Correction Factors for Electron Probe Microanalysis of Silicates, Oxides, Carbonates, Phosphates, and Sulphates," *Anal. Chem.* 42, 1408-1414 (1970).
28. J. G. Lion, "Synthesis and Stability Relations of Epidote, $\text{Ca}_2\text{Al}_2\text{FeSi}_3\text{O}_{12}(\text{OH})$," *Jour. Petrology* 14, 381-413 (1972).
29. G. Facca, "The Structure and Behavior of Geothermal Fields," in H. C. H. Armstead, ed., *Geothermal Energy, Review of Research and Development* (United Nations Educational, Scientific and Cultural Organization, Paris, 1973), pp. 61-69.
30. G. W. Grindley and P. R. L. Browne, "Structural and Hydrological Factors Controlling the Permeabilities of Some Hot-Water Geothermal Wells," in *Proceedings of the Second United Nations Symposium on the Development and Use of Geothermal Resources*, (Lawrence Berkeley Laboratory, Berkeley, California, 1976), Vol. 1, pp. 379-386.
31. California State Department of Conservation, Division of Oil and Gas, open-file report on Magmamax well No. 1.
32. J. H. Hill and C. J. Morris, "Sampling a Two-Phase Geothermal Brine Flow for Chemical Analysis" Lawrence Livermore Laboratory, Rept. UCRL-77544 (1975).
33. L. B. Owen, Lawrence Livermore Laboratory, private communication (1976).
34. G. Tardiff, Lawrence Livermore Laboratory, private communication (1976).

Appendix A

The Construction and Use of Activity Diagrams

Brief definitions of some geologic and chemical terms used in this paper are given for the convenience of the reader. (The construction and use of activity diagrams are based on the treatise by Hemley and Jones.²¹)

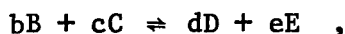
Metamorphism. The mineralogical and textural adjustment of solid rocks to physical and chemical conditions imposed at depth in the earth.

Hydrothermal Alteration. A type of metamorphism in which mineralogic and textural changes are brought about in rock by the percolation of hot solutions and gases through fractures and intergranular pore space.

Diagenesis. All of the chemical, physical, and biological changes, modifications, or transformations undergone by a sediment after its initial deposition and during the process of lithification, exclusive of metamorphism.

Activity. The concentration as modified by the effects of the solvent and solute on one another; the thermodynamic or effective concentration. Activity (a) is related to concentration (m) by the expression $a = \gamma m$, where γ is the activity coefficient.

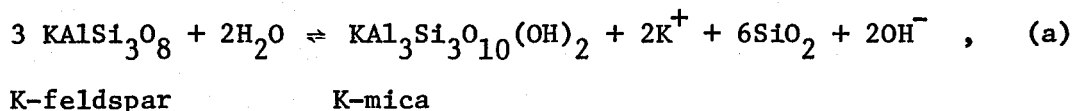
Equilibrium Constant. In the reaction

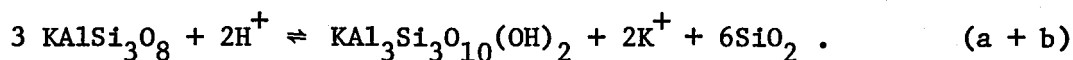


the equilibrium constant, K, is represented by the expression

$$K = \frac{(\text{activity of D})^d (\text{activity of E})^e}{(\text{activity of B})^b (\text{activity of C})^c} .$$

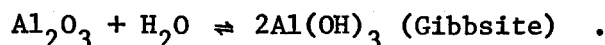
Hydrolysis. A reaction in which one of the decomposition products of water, either H^+ or OH^- , is selectively consumed thereby changing the H^+/OH^- ratio in solution. In the hydrolysis of a silicate mineral, an amount of cation, e.g., K^+ , chemically equivalent to the quantity of H^+ consumed must be released to the solution. The hydrolysis reaction between a silicate mineral and an aqueous solution is best illustrated as the sum of two equations (a and b):





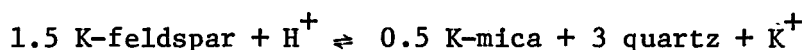
Note that reaction to the right consumes H^+ and releases K^+ .

Hydration. Hydration differs from hydrolysis in that it involves a chemical combination of water with another substance *without* the selective consumption of H^+ or OH^- . For example:



Hydrothermal alteration results from the reaction of minerals with the components of an aqueous solution. The process of hydrothermal alteration is complex, involving hydrolysis, hydration, and other reactions. In spite of the complexity of the process, field studies of hydrothermally altered terranes show recurring alteration patterns, i.e., certain mineral assemblages are characteristic of specific alteration zones. The correlation of field and experimental studies has indicated that (1) hydrolysis is quantitatively the most significant process involved in the alteration scheme and (2) the zonal alteration patterns reflect the degree of hydrolytic decomposition of silicate host rocks.

Hydrolysis reactions such as

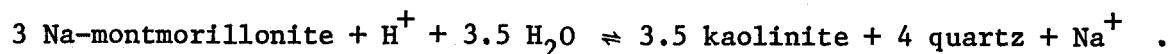
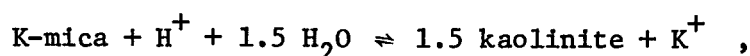
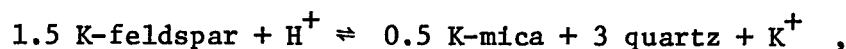


(same as a + b above) involve three solid phases and an aqueous phase. By convention, the activity of solids is taken as unity; therefore the equilibrium constant has the simple form

$$K = \frac{a\text{K}^+}{a\text{H}^+} \quad ,$$

and the system attains equilibrium at a specific $a\text{K}^+/a\text{H}^+$ ratio at a given temperature and pressure.

Laboratory investigations in the K_2O - and Na_2O - Al_2O_3 - SiO_2 - H_2O systems have dealt with a number of hydrolysis reactions that are important to the study of hydrothermal alteration. Some reactions investigated experimentally in the potassium-bearing and sodium-bearing systems are:



Note that in each reaction, the equilibrium constant can be expressed in terms of $a\text{K}^+/a\text{H}^+$ or $a\text{Na}^+/a\text{H}^+$. The experimental results for the four reactions in terms of temperature and the total KCl/HCl or NaCl/HCl ratio in solution are given in Figure A1. Quartz is present in the experimental assemblage, and total pressure is approximately 1 kbar.

In Fig. A2, the reaction curve data at 300°C for the systems K_2O - and $\text{Na}_2\text{O-Al}_2\text{O}_3\text{-SiO}_2\text{-H}_2\text{O}$ (dotted lines in Fig. A1) are combined to produce a mineral stability diagram for the five-component $\text{K}_2\text{O-Na}_2\text{O-Al}_2\text{O}_3\text{-SiO}_2\text{-H}_2\text{O}$

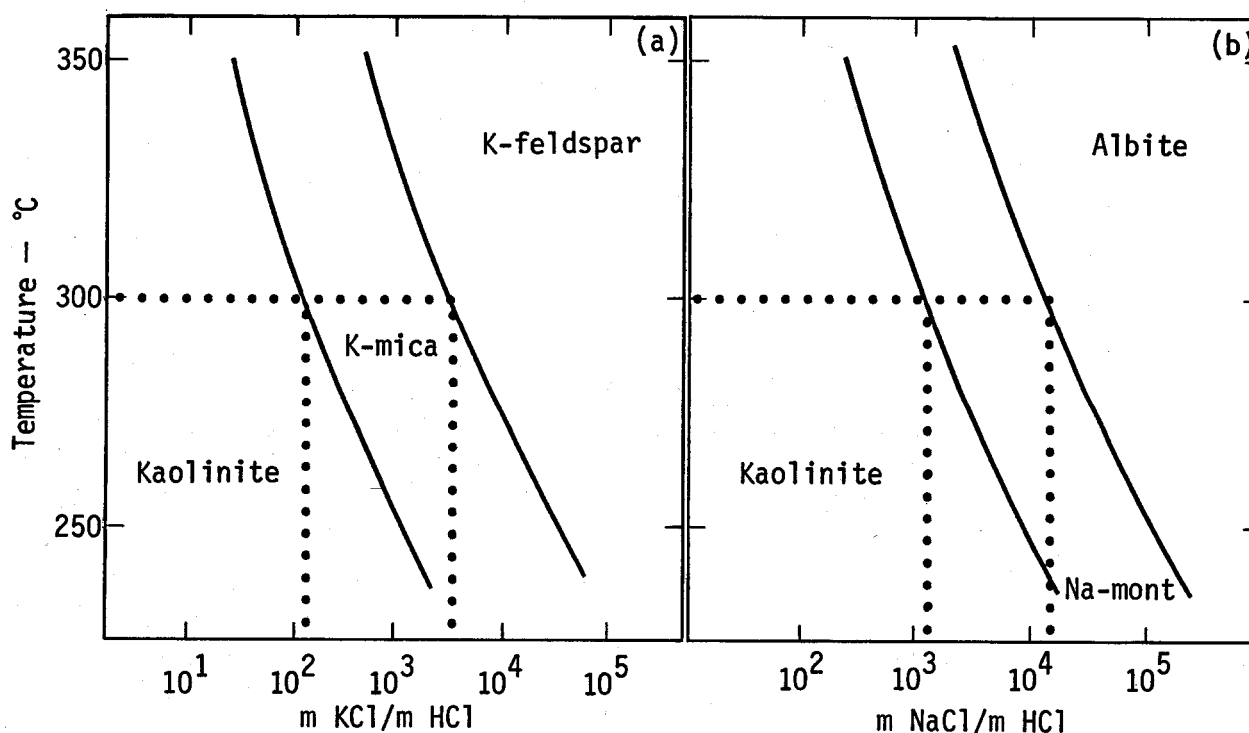


Fig. A1. Reaction curves for the systems $\text{K}_2\text{O-Al}_2\text{O}_3\text{-SiO}_2\text{-H}_2\text{O}$ and $\text{Na}_2\text{O-Al}_2\text{O}_3\text{-SiO}_2\text{-H}_2\text{O}$ from Hemley and Jones.²¹ Curves were established by approaching equilibrium in both directions, e.g., by placing feldspar in a solution with a KCl/HCl ratio within the K-mica field and alternatively by placing K-mica and quartz in a solution with a KCl/HCl ratio within the K-feldspar field. It should be noted that Hemley and Jones' data extends from 300 to 500°C and has been extrapolated to 250°C in this figure.

system. Figure A2 represents a slice in the three axis plot of $m\text{KCl}/m\text{HCl}-m\text{NaCl}/m\text{HCl}-T^\circ\text{C}$, which would incorporate all of the data available in Fig. A1. Note the similarity between Fig. A2 and Fig. 13b in the text. In Fig. 13, the coordinates are expressed in terms of activities that can be derived from concentration data in a number of ways. Helgeson (pp. 367-375)¹⁹ uses an extended form of the Debye-Huckel equation (the Delta approximation) for calculating activities.

It therefore follows that composition data for solutions in equilibrium with coexisting rock can be used to predict rock mineralogy. This has been done in Fig. 13 for Magmamax 1 and Sinclair 4.

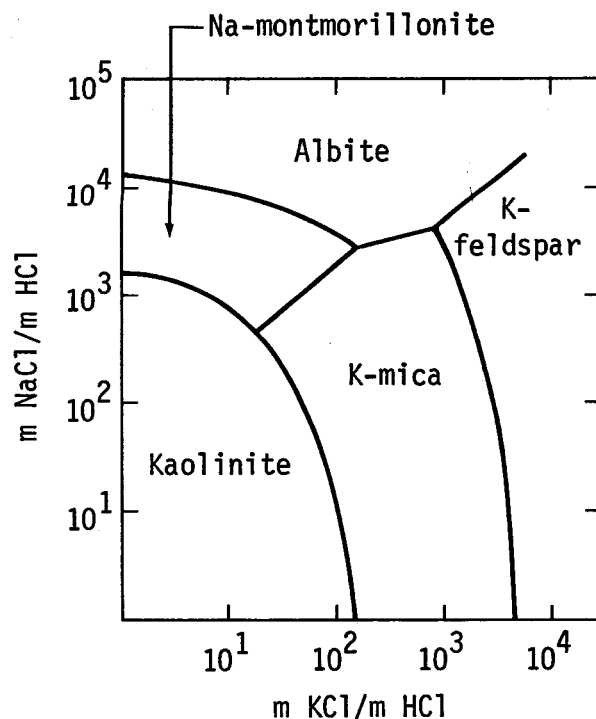


Fig. A2. Mineral stability relations in the system $\text{K}_2\text{O}-\text{Na}_2\text{O}-\text{Al}_2\text{O}_3-\text{SiO}_2-\text{H}_2\text{O}$ at 300°C and approximately 1 kbar.

Appendix B

Tables of Chemical Analyses

Table B1. Chemical analyses of chlorite from 4340-ft (1420-m) depth in Magmamax 2.

	C1 ^a	C2	C3	C4	C5	C6
SiO ₂	27.9	27.8	28.0	27.5	27.6	25.4
TiO ₂	0.0	0.0	0.0	0.1	0.0	0.1
Al ₂ O ₃	20.6	21.1	19.4	20.5	20.5	21.6
FeO	21.5	21.3	23.5	23.6	22.3	26.9
MgO	17.3	17.3	16.6	15.6	15.9	12.5
H ₂ O	12.6	12.2	12.3	12.4	13.1	13.3
Number of analytical points	5	4	6	5	4	8

^aNumbers C1 through C6 refer to nine individual chlorite grains from the sample. The chemical formula for chlorite C1 is:

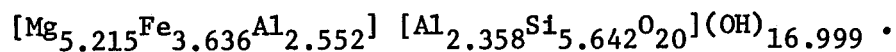
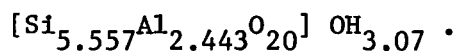
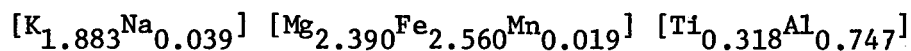


Table B2. Chemical analyses of biotite from 4340-ft (1420-m) depth in Magmamax 2.

	B1 ^a	B2	B3	B4	B5	B6	B7	B8	B9
SiO ₂	36.2	36.1	36.4	34.0	35.9	34.9	35.6	34.5	34.8
TiO ₂	2.8	3.2	0.8	2.8	0.9	2.4	3.3	2.5	1.7
Al ₂ O ₃	17.6	16.2	17.7	20.2	18.1	18.3	17.1	18.4	18.9
FeO	19.9	17.8	16.1	20.2	19.1	20.4	18.0	20.7	18.9
MgO	10.4	13.1	14.2	17.4	11.8	11.0	13.0	10.2	10.9
MnO ^b	0.1	0.1	0.1	0.1	0.1	0.1	0.1	0.1	0.1
K ₂ O	9.6	8.3	7.9	10.3	8.6	7.9	8.1	8.7	8.6
Na ₂ O	0.1	0.1	0.5	0.1	0.1	0.1	0.1	0.1	0.2
H ₂ O	3.3	5.1	6.3	4.9	5.4	4.9	4.7	4.8	5.8
Number of analytical points	5	6	6	6	3	3	2	4	3

^aNumbers B1 through B9 refer to nine individual biotite grains from the sample. The chemical formula for biotite B1 is:

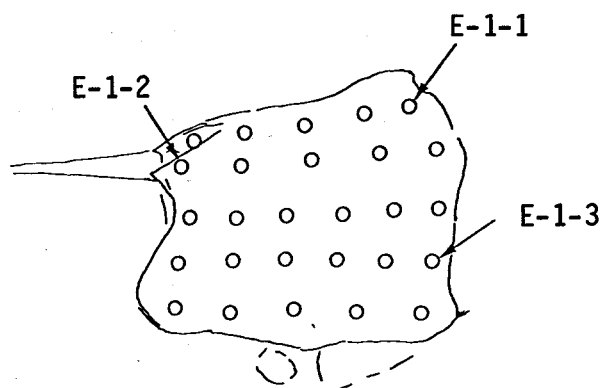
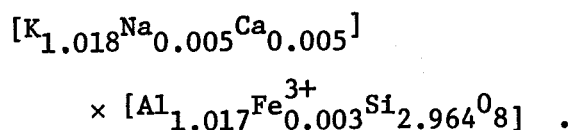


^bMnO content of 0.1 wt % represents the average of 12 analyses of random biotite grains. The range of values was from 0.08 to 0.2 wt %.

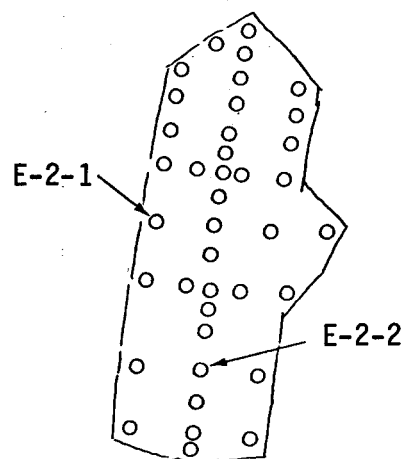
Table B3. Chemical analyses of feldspar from 4340-ft (1420-m) depth in Magmanax 2.

	F1 ^a	F2	F3
SiO ₂	63.9	63.9	64.1
Al ₂ O ₃	18.6	18.8	19.0
FeO	0.1	0.1	0.2
CaO	0.1	0.1	0.1
K ₂ O	17.2	17.7	17.8
Na ₂ O	0.6	0.5	0.4
Number of analytical points	5	4	5

^aNumber F1 through F3 refer to three individual feldspar grains from the sample. The chemical formula for feldspar F1 is :



Grain E-1, 27 points



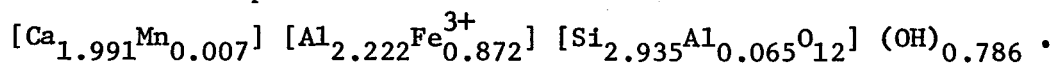
Grain E-2, 39 points

Fig. B1. Epidote grains contoured in Fig. 19. Open circles represent points of microprobe analyses. Arrows indicate points for which chemical analyses are given in Table B4.

Table B4. Selected epidote analyses from 4340-ft (1420-m) depth in Magmamax 2.

	E-1-1 ^a	E-1-2	E-1-3	E-2-1	E-2-2	E-1AV ^b	E-2AV ^c
SiO ₂	36.6	36.3	37.3	37.4	35.9	36.9	36.8
Al ₂ O ₃	24.2	20.6	21.8	22.3	21.2	22.4	22.0
Fe ₂ O ₃	14.5	19.9	18.2	16.8	18.3	17.2	17.2
TiO ₂	0.0	0.4	0.0	0.3	0.1	0.1	0.1
CaO	23.2	23.4	23.1	23.7	23.4	23.1	23.4
MnO	0.1	0.1	0.4	0.2	0.2	0.2	0.2
H ₂ O	1.4	0.0	0.0	0.0	0.9	0.1	0.3

^aNumbers E-1-1 through E-2-2 refer to analytical points on two individual grains of epidote. For instance, E-1-1 refers to point 1 on grain 1. The chemical formula for epidote E-1-1 is:



^bAverage of 27 analyses of epidote grain E-1.

^cAverage of 39 analyses of epidote grain E-2.

Appendix C

Porosity Measurements of Core Samples

Table C1. Porosity measurements of core samples from Woolsey No. 1 and State of California (SOC) No. 1.

Well	Sample Description	Depth, ft	Water corrected grain density ^a	Sample weight, g	Sample volume, ^b cm ³	Calculated porosity, %
Woolsey 1	Black shale	2568	2.847	8.433	3.700	19.9
Woolsey 1	Black shale	2568	2.847	12.877	5.875	23.0
Woolsey 1	Black shale	2568	2.847	13.380	6.030	22.1
Woolsey 1	Gray shale	2568	2.717	15.117	6.825	18.5
Woolsey 1	Gray shale	2568	2.717	15.345	6.810	17.1
Woolsey 1	Gray shale	2568	2.717	9.199	4.243	20.2
Woolsey 1	Lt. gray sandstone	2570	2.660	7.882	3.750	21.0
Woolsey 1	Lt. gray sandstone	2570	2.660	12.272	5.791	20.3
Woolsey 1	Lt. gray sandstone	2570	2.660	14.194	6.819	21.7
Woolsey 1	Gray shale	2589	2.755	9.233	4.200	20.2
Woolsey 1	Gray shale	2589	2.755	11.996	5.334	18.4
Woolsey 1	Gray shale	2589	2.755	7.859	3.570	20.1
Woolsey 1	Green-gray shale	3418	2.679	12.019	5.350	16.1
Woolsey 1	Green-gray shale	3418	2.679	7.855	3.445	14.9
Woolsey 1	Green-gray shale	3418	2.679	7.482	3.320	15.9
Woolsey 1	Green-gray shale	3419	2.684	10.848	4.900	17.5
Woolsey 1	Green-gray shale	3419	2.684	7.517	3.362	16.7
Woolsey 1	Green-gray shale	3419	2.684	7.835	3.530	17.3
SOC 1	Gray siltstone	4525	2.71	21.995	9.00	9.9
SOC 1	Green-gray siltstone	4592	2.75	20.833	8.20	7.5
SOC 1	Dk. gray siltstone	4842	2.76	17.007	6.60	6.5
SOC 1	Gray siltstone	4847	2.69	38.790	15.27	5.4
SOC 1	Gray siltstone	4847	2.67	20.806	8.30	6.2
SOC 1	Lt. gray siltstone	4848	2.69	29.415	11.82	7.4

^aGrain densities determined by means of a Beckman pycnometer.

^bVolumes determined by means of a Ruska mercury porometer.